Water Resources Research

RESEARCH ARTICLE

10.1029/2024WR038087

Water Table Fluctuations Control Nitrate and Ammonium Fate in Coastal Aquifers

Christian Roumelis[1], **Fabian Willert**[2], **Maria Scaccia**[1], **Susan Welch**[1], **Rachel Gabor**[3], **Jesús Carrera**[4,5], **Albert Folch**[5,6], **Miquel Salgot**[7], and **Audrey H. Sawyer**[1]

[1]School of Earth Sciences, The Ohio State University, Columbus, OH, USA, [2]Department of Geology, University of Vienna, Vienna, Austria, [3]School of Environment and Natural Resources, The Ohio State University, Columbus, OH, USA, [4]Institute of Environmental Assessment and Research, Barcelona, Spain, [5]Associated Unit: Hydrogeology Group (UPC-CSIC), Barcelona, Spain, [6]School of Civil and Environmental Engineering, Universitat Politècnica de Catalunya, Barcelona, Spain, [7]Soil Science Unit, University of Barcelona, Barcelona, Spain

Abstract Coastal aquifers experience water table fluctuations that push and pull water and air through organic-rich soils. This exchange affects the supply of oxygen, dissolved organic carbon (DOC), and nitrogen (N) to shallow aquifers and influences groundwater quality. To investigate the fate of N species, we used a meter-long column containing a sequence of natural organic topsoil and aquifer sediments. A fluctuating head was imposed at the column bottom with local, nitrate-rich groundwater (16.5 mg/L NO_3-N). We monitored in-situ redox potential and collected pore water samples for analysis of inorganic N species and DOC over 16 days. Reactive processes were more complex than anticipated. The organic-rich topsoil remained anaerobic, while mineral sediments beneath alternated between aerobic, when the water table dropped and sucked air across preferential flow paths, and anaerobic conditions, when the water table was high. A fluid flow and reactive transport model shows that when the water table rises into organic-rich soils, it limits the flow of oxygen, while the soils release DOC, which stimulates the removal of nitrate from groundwater by denitrification. At the end of the experiment, we introduced seawater to the column to mimic a storm surge. Seawater mobilized N and DOC from shallow soil horizons, which could reach the aquifer if the surge is long enough. These processes are relevant for groundwater quality in developed coastal areas with anthropogenic N sources, as climate change and rising seas will drive changes in water table and flood dynamics.

Plain Language Summary Coastal aquifers are subject to many hydrologic forces: rain, tides, floods, storm surges, and groundwater pumping, which cause groundwater levels to rise and fall. We find that these fluctuations control the fate of nitrogen species in groundwater, particularly nitrate, a common contaminant that impairs drinking water quality and causes harmful algal blooms when it enters coastal waters. As the water table rises and falls, the aquifer "breathes": it sucks air in and out of soils, allowing oxygen to reach sandy sediments below the carbon-rich topsoil. When the water table falls, oxygen enters soils and reacts with ammonium, which comes from the degradation of organic matter, to form nitrate. When the water table rises into topsoil, the source of oxygen is cut off. The saturated soils release organic carbon, which favors nitrate removal through denitrification. Seawater that enters soils during coastal flooding also flushes dissolved organic carbon and ammonium from soils and triggers nitrogen cycle reactions. Groundwater fluctuations thus drive substantial nitrogen transformations from the top of the soil to sandy sediments below, which influences the ultimate chemistry of shallow groundwater in coastal zones.

Key Points:

- Water table fluctuations pumped air across reducing topsoil, driving alternating aerobic and anaerobic conditions below
- Raising the water table in soils limited the supply of oxygen, added carbon, and sped up nitrate removal in groundwater
- In column experiment, a seawater flood flushed nitrogen and carbon from the vadose zone to the water table

Supporting Information:

Supporting Information may be found in the online version of this article.

Correspondence to:

A. H. Sawyer,
sawyer.143@osu.edu

Citation:

Roumelis, C., Willert, F., Scaccia, M., Welch, S., Gabor, R., Carrera, J., et al. (2025). Water table fluctuations control nitrate and ammonium fate in coastal aquifers. *Water Resources Research*, *61*, e2024WR038087. https://doi.org/10.1029/2024WR038087

Received 7 JUN 2024
Accepted 27 DEC 2024

Author Contributions:

Conceptualization: Jesús Carrera, Albert Folch, Audrey H. Sawyer
Data curation: Christian Roumelis, Maria Scaccia
Formal analysis: Christian Roumelis, Fabian Willert, Maria Scaccia
Funding acquisition: Christian Roumelis, Jesús Carrera, Albert Folch, Audrey H. Sawyer
Investigation: Christian Roumelis, Fabian Willert, Maria Scaccia, Audrey H. Sawyer
Methodology: Fabian Willert, Maria Scaccia, Susan Welch, Rachel Gabor, Jesús Carrera, Albert Folch, Miquel Salgot, Audrey H. Sawyer
Project administration: Audrey H. Sawyer

1. Introduction

Water tables in coastal aquifers respond to a variety of hydrologic forces that act onshore and offshore. Processes that act on land to control the water table include precipitation (Carretero & Kruse, 2012; Squeo et al., 2006) and groundwater pumping (Gejl et al., 2019; Jasechko et al., 2020). Processes that arise in the sea include waves, tides, and wind (Abarca et al., 2013; Goyetche et al., 2023; Greskowiak et al., 2023; Trglavcnik et al., 2018), coastal flooding (Cardenas et al., 2015; Heiss et al., 2022; Housego et al., 2021), and long-term sea level rise (Befus et al., 2020). These forces cause complex flow patterns that stimulate mixing and activate numerous biochemical reactions (Goyetche et al., 2022; Greskowiak et al., 2023). They also cause the water table to rise and fall, leading to abrupt variations of shallow moisture content. This wetting-drying cycle affects the supply of dissolved oxygen, carbon, and aerobic and anaerobic conditions throughout the soil profile (Haberer et al., 2012; Pal

Resources: Jesús Carrera, Albert Folch, Audrey H. Sawyer
Supervision: Susan Welch, Rachel Gabor, Audrey H. Sawyer
Validation: Christian Roumelis, Fabian Willert, Maria Scaccia, Susan Welch, Rachel Gabor, Jesús Carrera, Albert Folch
Visualization: Christian Roumelis, Audrey H. Sawyer
Writing – original draft: Christian Roumelis
Writing – review & editing: Rachel Gabor, Jesús Carrera, Albert Folch, Miquel Salgot, Audrey H. Sawyer

et al., 2010). When the water table rises and water fills the pores, it restricts the supply of oxygen from the atmosphere. If dissolved organic carbon (DOC) is also released from soils, aerobic respiration can quickly deplete oxygen, and microorganisms will respire other terminal electron acceptors such as nitrate (NO_3). When the water table falls, air is sucked into the vadose zone, and oxygen is reintroduced by advection into pores, where it drives aerobic respiration (Robertson & Groffman, 2007; Sinke et al., 1998). We conjecture that this fluctuation between oxic and anoxic conditions may regulate nitrogen (N) transport and fate in shallow groundwater (Cirmo & McDonnell, 1997; Hefting et al., 2004), particularly in coastal zones that are subject to frequent hydrologic changes.

The fate and transport of N is important in coastal environments, which tend to be densely populated with long histories of land use change and anthropogenic N contamination (Rivett et al., 2008) from fertilizers and wastewater (Almasri & Ghabayen, 2008; Johannes, 1980; Kwon et al., 2021). Coastal aquifers are particularly vulnerable to N pollution due to their shallow water tables (Chang & Clement, 2013; Heaton et al., 2012). Accumulations of NO_3 are linked to negative environmental and health issues (de Voogt, 2017). Studies in Asia (Chen et al., 2007), America (Burkart & Stoner, 2008; Isla et al., 2018; Nolan, 2001; Spalding & Exner, 1993), and Europe (Heaton et al., 2012; Mostaza-Colado et al., 2018; Strebel et al., 1989) have shown significant NO_3 pollution in shallow aquifers. More recently, Abascal et al. (2022) examined 292 locations around the globe and found NO_3 pollution in groundwater to be increasing with the greatest concentrations in the Mediterranean and South Asian regions. The discharge of NO_3-rich groundwater to the coast affects marine surface waters. Because primary production is often N-limited in marine waters, new N loads from groundwater can cause eutrophication and degrade coastal ecosystems such as estuaries and reefs (Howarth & Marino, 2006).

NO_3 is both a product and reactant in a number of biogeochemical processes that occur in soils and groundwater (Cirmo & McDonnell, 1997; Rivett et al., 2008). Under oxic conditions, microbes produce NO_3 through the oxidation of ammonium (NH_4) (Shah & Coulman, 1978). Under anoxic conditions, microbes reduce NO_3 to N_2 gas through denitrification (Rivett et al., 2008). Denitrification is the primary process that removes NO_3 from groundwater and requires a source of labile organic carbon (Baker & Vervier, 2004). NO_3 and NH_4 can also be assimilated by microbes and plants, and NH_4 can also be oxidized through anammox, but this process is purported as a non-dominant reaction pathway in sandy coastal aquifers (Smith & Duff, 1988). The rates of nitrification and denitrification are strongly influenced by the water table, which regulates the supply of oxygen from soil gas and organic carbon from soil organic matter (Kliewer & Gilliam, 1995).

Column experiments have been widely used to examine the fate and transport of redox-sensitive elements such as carbon and N (Fierer & Schimel, 2002; Rodríguez-Escales et al., 2016), oxygen (Haberer et al., 2012), and arsenic (Tran et al., 2022). In columns, fluid flow rates and saturation states can be controlled to explore the implications for biogeochemical transport. For example, Rezanezhad et al. (2014) examined the geochemical and microbial responses of two identical soil columns with a stable and fluctuating water table. They found that a fluctuating water table transported iron, manganese, phosphorus, sulfur and magnesium to deeper depths and stimulated microbial growth and activity compared to a static water table. More recently, Zhang and Furman (2021) used soil columns to investigate N transformations in the capillary fringe in a homogeneous sandy medium and found water movement to be significant to N removal in the capillary fringe. While column studies abound in the literature, relatively few examine the impact of a fluctuating water table (Holocher et al., 2002; Jost et al., 2015; Rühle et al., 2015), and even fewer examine these processes in heterogeneous media.

Natural soils have varying vertical distributions of minerals, organic content, and microbial communities that influence biogeochemical reactions at different depths, making it important to account for vertical heterogeneity in column experiments. Soil organic matter in particular tends to decrease exponentially with depth (Pabich et al., 2001) and acts as a source of DOC to groundwater. DOC is often a limiting reactant for denitrification in aquifers (Sobczak et al., 2003), and high rates of denitrification have been observed in reducing environments in organic-rich materials (Hill et al., 2000). Note that this view implicitly assumes oxygen is effectively consumed within the vadose zone (see discussion by Arora et al., 2019). Yet, hydrogeologists often assume that shallow groundwater remains oxic through oxygen diffusion across the vadose zone (see discussion in Chapter 9 of Appelo & Postma, 2004). In fact, this question of oxygen fluxes motivated experiments by Haberer et al. (2012, 2015) to show that water table fluctuations and trapped air could explain oxygen transfer across the capillary fringe barrier, provided oxygen was available above. Their experiments were conducted in a porous matrix formed by glass beads and did not consider the added effect of soil carbon sources. Thus, experiments involving natural soil sequences can shed new light on soil, vadose zone, and aquifer interactions, especially when it comes to redox reactions, which control the N cycle, among others.

In this context, our initial goal was to use column experiments and numerical models to investigate how water table fluctuations, which bring NO_3-rich groundwater in contact with organic carbon in shallow soils, influence the fate and transport of N in a coastal aquifer. We found that as the water table rises and falls, it pushes and pulls air through preferential flow paths in the organic-rich topsoil—the aquifer “breathes”—and the combined effects of alternating oxygen and carbon supplies drive changes in N chemistry. We also investigated the effect of a seawater flood, as these events will become more common as sea level rises and should elicit a different effect on N transport compared to flooding from the bottom. We used numerical models to frame experimental observations. This study is unique because: (a) the column materials have greater organic matter content near the surface, reflecting a typical soil sequence, and come from real coastal sediments, (b) we simulated different time scales and repeated cycles of water table fluctuations, and (c) we used natural groundwater with elevated NO_3 concentrations pumped directly from the local unconfined aquifer, which ensures a more complex pool of dissolved organic matter for studying carbon-sediment interactions in the column.

Figure 1. Aerial image of the field site on Mediterranean coast (Mataró, Spain). Box A shows the floodplain area where soils were collected near the outlet of an ephemeral stream along the coast. The watershed and underlying aquifer are strongly influenced by anthropogenic activities (Folch et al., 2020).

2. Materials and Methods

2.1. Site Description

Sediment, soil, and groundwater for the column study were supplied from an unconfined alluvial aquifer on the Mediterranean coast where groundwater is contaminated with NO_3. The site lies approximately 30 km northeast of Barcelona near the outflow of the ephemeral Argentona stream, which flows following large precipitation events (Folch et al., 2020) (Figure 1). The catchment hosts a mixture of industrial operations, farmland, and densely populated towns. The site is well-suited for examining N transport in an anthropogenically impacted coastal floodplain aquifer with sandy soils.

The site has been the focus of detailed hydrogeologic investigations to understand submarine groundwater discharge and seawater intrusion, but most observations have targeted the confined aquifer layers, which provide a freshwater source for local towns and agriculture (Folch et al., 2020; Martínez-Pérez et al., 2022; Palacios et al., 2020). The layered aquifer system is approximately 20 m thick and consists of well-sorted quaternary sand units separated by relatively thin, decimeter-thick silt and clay layers (Folch et al., 2020). The water table lies in the shallowest sandy layer, which is approximately 7 m thick. Bulk conductivity generally increases in the deeper layers (Martínez-Pérez et al., 2022; Palacios et al., 2020). NO_3-N concentrations observed by Martínez-Pérez et al. (2022) were greatest in the shallow aquifer (15.4 mg/L–21.3 mg/L) and decreased with depth in the intermediate (0.4 mg/L–10 mg/L) and deep semi-confined aquifer layers (0.1 mg/L–2.2 mg/L). Several biogeochemical reactions occur in the fresh-seawater mixing zone that affect N compounds in the aquifer (Goyetche et al., 2022), but the importance of soil and reactive transport processes near the water table has not been investigated.

2.2. Soil Selection and Column Construction

The column was constructed of PVC pipe (30.48 cm inner diameter and 105 cm length) and packed with sediments collected from the unconfined alluvial aquifer and the vadose zone between April 28-29, 2022 (Figure 2). The column stratigraphy was intended to represent a simplified version of a natural soil profile with 4 layers to represent the transition from organic-rich surface soils to inorganic aquifer sands. A soil trench was dug on site, and three representative depth intervals were selected for integrated sampling: 100-60 cm, characterized as uniform sand with little to no organic material (mineral I); 60-30 cm, characterized as visually uniform sand with greater organic matter content (mineral II); and 10–30 cm, characterized as dark organic soil with sparse

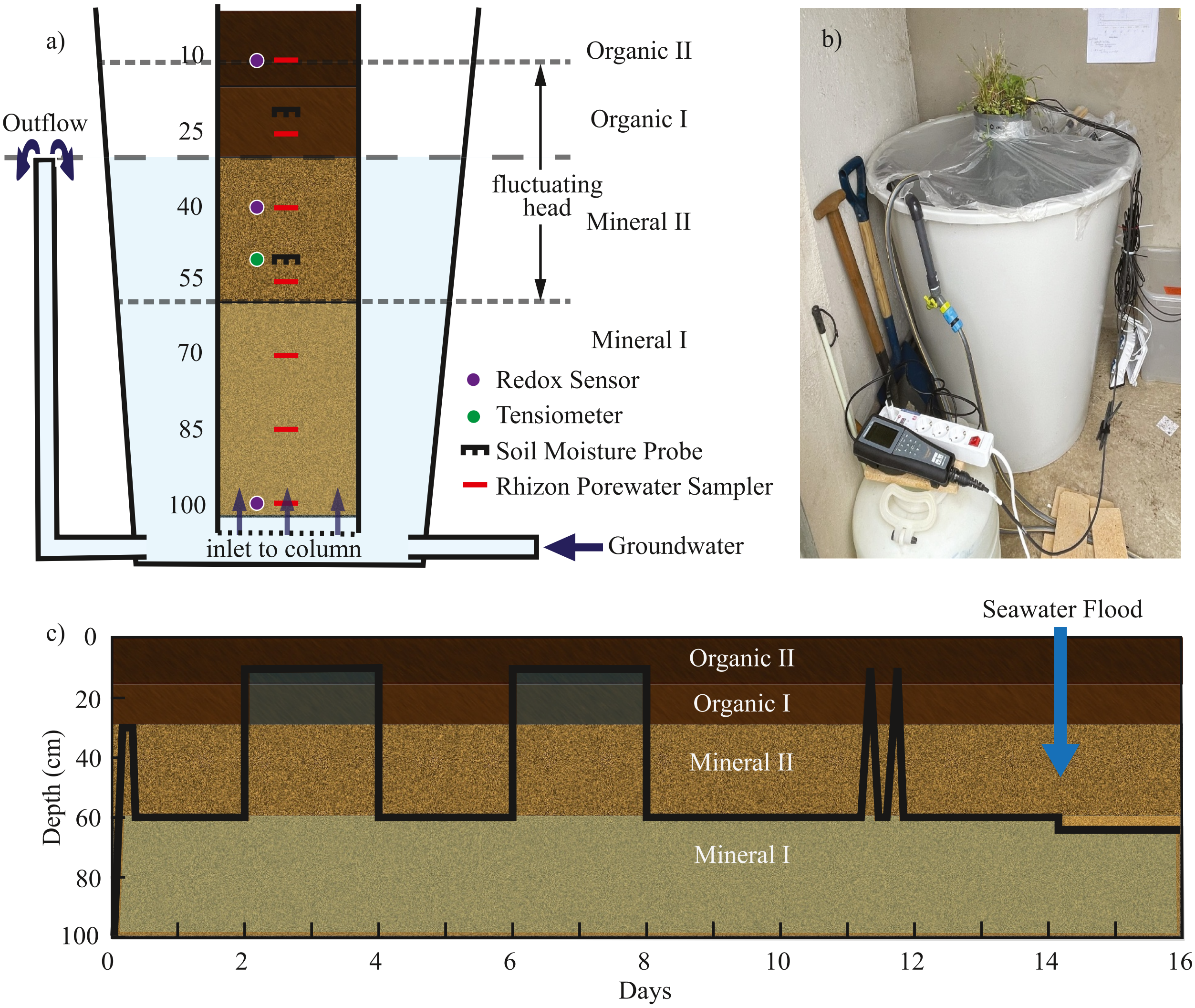

Figure 2. (a) Schematic of experimental setup. (b) Photograph of experimental setup. (c) Schedule of water table fluctuations and seawater overtopping event. Two 4-day water table cycles were chosen to allow ample time for water to react with soils and alter water chemistry. Two rapid water table cycles were performed on day 11 to assess the impact of fast wetting and drying on dissolved organic carbon and N transport. In the seawater overtopping event, the water table was intended to remain stable at a depth of 60 cm but inadvertently fell to 65 cm.

vegetation and debris such as roots and leafy material (organic I). Material from each interval was placed into its own separate container. Roots, debris, and large objects were removed, and the material was churned to homogenize it. The motivation for creating these homogenized zones was to maintain the overarching trends in soil characteristics (particularly depth-decaying organic matter content) while packing a rather large column with samplers and sensors. Typically, column studies that examine water table fluctuations are performed with entirely homogeneous sediments or glass beads (e.g., Pronk et al., 2020; Rezanezhad et al., 2014; Rühle et al., 2015; Williams & Oostrom, 2000). The approach taken here achieves a more natural but well-characterized soil sequence.

Before loading material into the column, a thin layer (<5 cm) of store-bought pea gravel was washed with fresh groundwater and placed in the bottom to maintain uniform flow to the column base. The lower 40 cm were then filled with homogenized inorganic sand material from the 100-60 cm depth interval from the trench site (mineral I). The next 30 cm were filled with homogenized organic sand material from the 60-30 cm depth interval (mineral II). The next 15 cm were filled with homogenized soil collected from 15 to 30 cm deep (organic I). For the uppermost 15 cm, a plug of topsoil with natural vegetation was removed from alongside the soil pit and placed on top of the three homogenized layers (organic II) (Figure 2). We therefore assume the approximate root depth in the column was 15 cm. Soil samples were collected from the three homogenized materials and the intact surface layer at the time of column construction and kept frozen until analysis for total organic carbon content and grain size.

While adding the organic and mineral layers, seven Rhizon pore samplers (Rhizosphere MacroRhizon) were placed at 15 cm intervals from 100 to 10 cm deep (Figure 2). A spacing of 15 cm was chosen because it was estimated that the Rhizons would retrieve pore water from an approximately 10-cm thick volume, and we sought to maintain discrete sample volumes. Two soil moisture probes (Teros 12 soil moisture, temperature, and electrical conductivity) were placed at 20 and 50 cm depths. A tensiometer (Teros 32, soil water potential and temperature) was also inserted at a 45-degree angle to 50 cm depth. Both the soil moisture probes and tensiometer were connected to a digital data logger that recorded measurements every 5 min. A meter-long redox probe (SWAP soil redox probes, ORP custom-made) was inserted into the column with electrodes at 10 cm, 40 cm, and 100 cm (Figure 2). The corresponding AgCl reference electrode was placed in the unsaturated top-soil layer. The redox sensors and reference electrode were attached to a Campbell logger that recorded measurements throughout the experiment. The entire soil column was placed into a large tank with a siphon to control hydraulic head at the base of the column (Figure 2).

Each day for at least 4 hr, groundwater was produced from an on-site well and circulated through the tank that was used to fill the column. The well has a total depth of 15 m and is screened within the unconfined aquifer. To minimize oxygen exchange between the groundwater in the tank and atmosphere, a plastic sheet was secured over the tank and around the column sides and sealed with tape (Figure 2b). Care was also taken to minimize light transfer into the tank and thus algal growth. A YSI multiparameter water quality probe continuously recorded the pH, ORP, temperature, electrical conductivity, and dissolved oxygen of the tank water throughout the experiment, and care was taken to ensure minimal fluctuation in recorded parameters, including dissolved oxygen.

2.3. Experimental Design

Column experiments were conducted in May of 2022. The schedule of imposed water level fluctuations was chosen to explore two timescales of change: multiple days and hours (Figure 2). The two timescales were chosen to explore what happens when there is ample time for oxygen consumption (multi-day) and when the fluctuations outpace oxygen dynamics (hour), as oxygen is a key factor in nitrification and denitrification. The imposed fluctuations are necessarily simplistic compared to natural fluctuations in unconfined aquifers, due in part to the limited height of the column. They are also intentionally simplistic in one specific aspect: we imposed rapid changes in water level, followed by periods with no change. This discontinuous signal is unlike a smoothly varying tidal signal, but it is ideal for isolating chemical reactions from transport processes during times when the water table is stationary. We also note that coastal aquifers are subject to many disturbances, including abrupt ones due to groundwater pumping. Thus, the experimental design is advantageous for revealing reactive N transport processes under scenarios where the water table moves vertically through gradients in soil organic content, a key goal of the study that does not depend on the driving force of the fluctuation.

The soil column was initialized by raising the water table to 30 cm below the soil surface to saturate the sandy aquifer layers and then lowering the water level to 60 cm below the surface to develop a naturally drained profile (Figure 2). The first 2-day fluctuation cycle began on day 2 by raising the water level to 10 cm depth and holding it constant for 2 days (Figure 2c). The water level was then lowered again to 60 cm for 2 days. A second 2-day cycle was then imposed to examine whether successive wetting events behaved similarly or whether differences might occur due to, for example, microbial dynamics or initial conditions. On day 11, the water table was quickly raised and lowered twice on the same day to simulate tidal events of faster frequency (Figure 2). On day 14, the top of the column was flooded with seawater collected on site to simulate inundation that occurs during storm surges.

Over the 16-day experiment, loggers were programmed to record redox potential every 10 min, while soil moisture and matric potential were recorded every 5 min. Following the seawater flood on day 14, soil moisture sensors at 20 and 50 cm recorded apparently large volumetric water contents that exceeded observed saturation values on days when the water table was elevated above the sensors, which we attribute to the increased electrical conductivity of seawater. Therefore, we applied a correction to the 20 cm sensor using a modified version of Archie's Law for unsaturated soils, where the logarithm of volumetric water content varies linearly with the logarithm of the ratio of bulk electrical conductivity (from the sensor itself) to fluid electrical conductivity (from the nearest porewater samplers). The same correction was attempted for the sensor at 50 cm, but there was no clear relationship between volumetric water content, bulk electrical conductivity, and fluid electrical conductivity over the narrow range of near-saturated conditions there, so data were truncated following the seawater flood.

2.4. Porewater Sampling

One round of pore water samples (a sample from each depth) was collected on days with a static water level, and three rounds were collected on days with a rising or falling water table—a round before, during, and after the fluctuation. These intervals were chosen to minimize extracted volumes and disturbance to geochemical profiles while capturing the times when the chemistry would be expected to change most rapidly.

Samples were collected from Rhizon samplers (pore size of 0.15 μm) into 60-mL syringes. The volume is equivalent to the water content in a saturated disk of column material with height of <0.3 cm. Upon collection, samples were filtered again to 0.22 μm using Fisherbrand polyethersulfone (PES) syringe filters and split into three designated aliquots: 15 mL for nutrient analysis, including NO_3-N, NO_2-N, and NH_4-N (collected in unacidified falcon tubes), 20 mL for DOC and fluorescence analysis of DOM (collected in pre-combusted amber glass vials), and 15 mL for analysis of manganese, iron, and aluminum (collected in unacidified falcon tubes). The remaining 10 mL were used to measure fluid conductivity, pH, temperature, and ORP immediately in the field with a Myron Ultrameter II (Figure S1 in Supporting Information S1). Collected samples were placed on ice until they were transported to the Spanish National Research Council (CSIC) at the end of each day, where they were stored in a dark, refrigerated room at 4 degrees Celsius for approximately 2 weeks until they were transported on ice to Ohio State University (OSU) for rapid analysis. More details on sampling procedures are available in Roumelis (2023).

2.5. Porewater Analyses

All water sample analyses except for iron and manganese were run at OSU facilities. N-species (NO_3-N, NO_2-N, NH_4-N) were measured using the Skalar SAN ++ nutrient analyzer. Samples were initially diluted by 1:5 and then 1:10 if the measurements exceeded the standard curve. The typical detection limit for NO_2-N was 0.001 mg/L. Detection limits for NH_4-N and NO_3-N were 0.006 mg/L and 0.008 mg/L, respectively, estimated as twice the standard deviation of replicate analyses of low standards. DOC concentrations were measured as non-purgable organic carbon using a Total Organic Carbon Analyzer (Shimadzu Inc.). Samples collected after the seawater infiltrations experiment on 8 June 2022 were diluted according to field measurements of specific fluid conductivity to ensure the carbon analyzer was not damaged by high salt concentrations. Manganese, iron and aluminum were run using inductively coupled plasma optical emission spectroscopy at CSIC in Barcelona, Spain. The estimated error was <2% and precision 1%. A subset of samples was also analyzed for chloride and other major anions using ion chromatography on a Dionex ICS 2100.

2.6. Soil and Sediment Analyses

Sediment samples were analyzed for oxidizable carbon content using the Walkley and Black method (De Vos et al., 2007) and organic matter through combustion at 550 degrees Celsius.

Hydraulic conductivity was estimated through two approaches. We used the Hazen method to estimate the saturated hydraulic conductivity of each soil layer from grain size analysis (Hazen, 1911). We also estimated an equivalent saturated hydraulic conductivity for the layered column system using infiltration rates recorded during the seawater flood event. Specifically, during the seawater flood, water was added to the top of the column to visually maintain saturated but not ponded conditions. The volume and time were recorded for each seawater addition, and the resulting plot of infiltration rate versus time was used to calculate the saturated hydraulic conductivity according to the Green-Ampt solution.

2.7. Numerical Model

We used the Richards Equation to solve for variably saturated single-phase flow in the vertical direction:

$$\rho\left(\frac{C_m}{\rho g}+S_e S\right)\frac{\partial P}{\partial t}=\nabla\cdot\rho\left(\frac{k_s}{\mu}k_r\left(\nabla P-\rho\vec{g}\right)\right) \tag{1}$$

where ρ is water density [kg/m^3], S_e [-] is effective saturation ($S_e = \theta - \theta_r/\theta_s - \theta_r$, where θ is volumetric water content [-] and subscripts "*s*" and "*r*" denote saturated and residual values), C_m is the specific moisture capacity [1/m] calculated from S_e according to the Van Genuchten model, S is the storage coefficient [1/Pa], k_s is saturated permeability [m^2] derived from the hydraulic conductivity, μ is dynamic viscosity [Pa·s], k_r is relative permeability [-] according to the Van Genuchten model, g is gravitational acceleration [m/s^2], and P is pressure [Pa].

For unsaturated conditions ($S_e < 1$):

$$S_e = \left(1 + \left|\alpha \frac{P}{\rho g}\right|^n\right)^{-m} \tag{2}$$

α, m, and n are the Van Genuchten parameters, which were approximately constrained using observations of P and θ from soil moisture sensors in the Mineral II layer (Figure 2, Table 1). Because other layers lacked paired tensiometer and soil moisture sensors to constrain spatial variations in Van Genuchten parameters, we held them constant. We did assign different values of porosity (θ_s) in the mineral and organic layers based on measurements at the two soil moisture sensors (Figure 2, Table 1).

Using water fluxes and effective saturation from the solution to Equation 1, we then solved for chemical transport of chloride, DOC, dissolved oxygen (O_2), ammonium (NH_4), nitrate (NO_3), and nitrite (NO_2) in two dimensions according to the advection-dispersion-reaction equation in variably saturated porous media:

$$\frac{\partial(\theta c_i)}{\partial t} + \frac{\partial\left(\rho_{\mathrm{bd}} c_{\mathrm{s},i}\right)}{\partial t} + \frac{\partial\left(\theta_g c_{\mathrm{g},i}\right)}{\partial t} = \nabla \cdot (D_i \nabla c_i) - \nabla \mathrm{q} c_i + \theta R_i + Q_{\mathrm{ex},i} \tag{3}$$

where c_i [mol/m^3], $c_{\mathrm{s},i}$ [mol/kg], and $c_{\mathrm{g},i}$ [mol/m^3] are the concentrations of the ith chemical compound in the aqueous, solid phase, and gas phases, respectively, ρ_{bd} is dry bulk density [kg/m^3], θ_g is the volumetric gas content ($\theta_s - \theta$), D_i is the effective diffusion coefficient [m^2/s], q is water flux [m/s], R_i is the source or sink due to aqueous-phase reactions (Γ) involving the ith species [mol/m^3/s], and $Q_{\mathrm{ex},i}$ is any additional source or sink for the ith species [mol/m^{3}s]. For all dissolved species, the effective diffusion coefficient was defined as $\theta/\tau\ D_L$, where tortuosity (τ) was estimated using the Millington and Quirk model ($\tau = \theta^{-7/3}\ \theta_{\mathrm{s}}{}^2$) and D_L is the free diffusion coefficient in liquid. In the case of oxygen only, the effective diffusion coefficient also included a term for enhanced diffusion in the gas-filled pores, where $D_{\mathrm{i}} = \theta/\tau\ D_{\mathrm{L}} + \theta_{\mathrm{g}}/\tau_{\mathrm{g}}\ \kappa_{\mathrm{g},i}\ D_{\mathrm{g}}$, and $\tau_{\mathrm{g}} = \theta_{\mathrm{g}}{}^{-7/3}\ \theta_s{}^2$. Gas exchange with air-filled pores was treated as an instantaneous (equilibrium) exchange process ($c_{\mathrm{g},i} = \kappa_{\mathrm{g},i}\ c_{\mathrm{i}}$, where $\kappa_{\mathrm{g},i}$ is Henry's constant expressed in terms of concentration [-]). This equilibrium allows us to incorporate gas diffusion by enlarging the value of D_{i} in Equation 3 through the contribution of D_{g} (Table 1). We used a mixed type boundary condition with large conductance at the top of the column to represent efficient oxygen exchange across the soil-air interface, and we set the external concentration of oxygen such that $c_{\mathrm{g},i}\kappa_{\mathrm{g},i} = 10$ mg/L. As a result, modeled oxygen concentrations at the top boundary remain near saturation (10 mg/L).

For O_2, NH_4, NO_3, NO_2, and DOC, R_i included terms for nitrification, aerobic respiration, and two-step denitrification, which were treated according to Monod kinetics (Table 2):

$$R_{\mathrm{O}_2} = -\mathrm{x}\Gamma_{\mathrm{AR}} - \Gamma_{\mathrm{NIT}} \tag{4}$$

$$R_{\mathrm{NH}_4} = -0.5\Gamma_{\mathrm{NIT}} + \mathrm{y}\Gamma_{\mathrm{AR}} + \mathrm{y}\Gamma_{\mathrm{DN1}} + \mathrm{y}\Gamma_{\mathrm{DN2}} \tag{5}$$

$$R_{\mathrm{NO}_3} = 0.5\Gamma_{\mathrm{NIT}} - 2\mathrm{x}\Gamma_{\mathrm{DN1}} \tag{6}$$

$$R_{\mathrm{NO}_2} = 2\mathrm{x}\Gamma_{\mathrm{DN1}} - \frac{4}{3}\mathrm{x}\Gamma_{\mathrm{DN2}} \tag{7}$$

$$R_{\mathrm{DOC}} = -\mathrm{x}\Gamma_{\mathrm{AR}} - \mathrm{x}\Gamma_{\mathrm{DN1}} - \mathrm{x}\Gamma_{\mathrm{DN2}} \tag{8}$$

Oxygen was treated as an inhibitor for denitrification.

In the case of NH_4, we included instantaneous (equilibrium) reversible sorption ($c_{\mathrm{s},i} = \kappa_{\mathrm{s},i}\ c_{\mathrm{i}}$) with a sorption isotherm that varied exponentially with chloride concentration (a proxy for salinity):

Table 1
Numerical Model Parameters and Definitions

	Definition	Value
Parameter		
D	Free diffusion coefficient in liquid	5×10^{-8} m^2/s
D_g	Free diffusion coefficient in gas	3×10^{-5} m^2/s (2×10^{-5}–2×10^{-4})
g	Gravitational acceleration	9.81 m/s^2
k_s	Saturated permeability	1.24×10^{-11} m^2 (organic I), 1.63×10^{-11} m^2 (organic II) 2.73×10^{-10} m^2 (mineral I), 1.26×10^{-11} m^2 (mineral II)
m	Van Genuchten parameter	0.6
n	Van Genuchten parameter	2.5
S	Storage coefficient	1.66×10^{-9} Pa^{-1} (organic), 1.56×10^{-9} Pa^{-1} (mineral)
$x{:}y$	C:N production ratio from mineralization of OM	15:1 (10:1–25:1)
α	Van Genuchten parameter	4 m^{-1}
β	Coefficient for linear sorption isotherm, NH_4	−2
$\kappa_{s,i\ 0}$	Coefficient for linear sorption isotherm, NH_4	2 mL/g
μ	Dynamic viscosity	0.001 Pa-s
ρ	Water density	1,000 kg/m^3
ρ_g	Grain density	2,600 kg/m^3
θ_s	Porosity	0.40 (organic), 0.45 (mineral)
θ_r	Residual volumetric water content	0.05 (organic), 0.05 (mineral)
a	Carbon mass transfer coefficient	10^{-9} s^{-1}
f_{som}	Fraction of soluble organic matter	0.0801 (organic I), 0.0889 (organic II), 0.0033 (mineral I), 0.0062 (mineral II)
B	Biomass	10^{-4} mol/m^3
K_d	Mass-transfer distribution coefficient for carbon	2 m^3/kg
k_{I,O_2}	Oxygen inhibition constant	0.18 mg/L (0.1–2)
$k_{s,DOC}$	Half saturation constant, DOC	6 mg/L
k_{s,NH_4}	Half saturation constant, NH_4	0.2 mg/L
k_{s,NO_3}	Half saturation constant, NO_3	1.6 mg/L
k_{s,NO_2}	Half saturation constant, NO_2	0.1 mg/L
k_{s,O_2}	Half saturation constant, O_2	3 mg/L
v_{AR}	Maximum specific aerobic respiration rate	2.75 hr^{-1} (1–10)
v_{NIT}	Maximum specific nitrification rate	7.5 hr^{-1} (1–10)
v_{DN1}	Maximum specific denitrification rate, step 1	3.75 hr^{-1} (0.5–5)
v_{DN2}	Maximum specific denitrification rate, step 2	8.9 hr^{-1} (1–10)
Boundary conditions		
q_{sw}	Infiltration rate during flood	1.8×10^{-5} m/s
$c_{DOC,sw}$	DOC in seawater flood	0.9 mg/L
$c_{NO_3,sw}$	NO_3-N in seawater flood	0.13 mg/L
$c_{NH_4,sw}$	NH_4-N in seawater flood	0.01 mg/L
$c_{NO_2,sw}$	NO_2-N in seawater flood	0.003 mg/L
$c_{O_2,sw}$	O_2 in seawater flood	10 mg/L
$c_{Cl,sw}$	Cl in seawater flood	20.6 g/L
$c_{DOC,gw}$	DOC in groundwater at base (open boundary)	1.46 mg/L
$c_{NO_3,gw}$	NO_3-N in groundwater at base (open boundary)	16.5 mg/L

Table 1
Continued

	Definition	Value
$c_{\mathrm{NO_2,gw}}$	NO_2-N in groundwater at base (open boundary)	0.05 mg/L
$c_{\mathrm{NH_4,gw}}$	NH_4-N in groundwater at base (open boundary)	0.01 mg/L
$c_{\mathrm{O_2,gw}}$	O_2 in groundwater at base (open boundary)	0.77 mg/L
$c_{\mathrm{Cl,gw}}$	Cl in groundwater at base (open boundary)	75 mg/L

Note. Ranges for the 7 parameters that we randomly varied to improve model fit are shown in italics with parentheses. Unless specified otherwise, parameter values were uniform throughout the column.

$$\kappa_{\mathrm{s},i} = \kappa_{\mathrm{s},i0} \exp\left(-\beta \frac{c_{\mathrm{Cl}}}{c_{\mathrm{Cl,sw}}}\right) \tag{9}$$

Note that, neglecting changes in ρ_{bd}, the second term on the left side of Equation 3 is:

$$\frac{\partial(\rho_{\mathrm{bd}} c_{\mathrm{s},i})}{\partial t} = \rho_{\mathrm{bd}} \kappa_{\mathrm{s},i}(c_{\mathrm{Cl}}) \left(\frac{\partial \mathrm{c}_i}{\partial t} - \frac{\beta \mathrm{c}_i}{c_{\mathrm{Cl,sw}}} \frac{\partial \mathrm{c}_{\mathrm{Cl}}}{\partial t}\right) \tag{10}$$

where the last term acts as a source of NH_4 due to desorption at moving salinity fronts (implemented in the numerical model as a source term, $Q_{\mathrm{ex,NH_4}}$).

To represent a kinetically limited source of DOC from soils and sediments, we included a reversible first-order mass-transfer reaction (Jardine, 1992):

$$Q_{\mathrm{ex,DOC}} = \rho_{\mathrm{bd}} a \left(f_{\mathrm{SOM}} - K_d c_{\mathrm{DOC}}\right) \tag{11}$$

where a is the carbon mass transfer coefficient [1/s], f_{som} is soluble organic matter content [kg/kg] (here, assumed equal to the measured organic matter content in organic layers and half the organic matter content in mineral layers), and K_{d} is the distribution coefficient between SOM and DOC [m^3/kg] (Table 1). This formulation assumes that soil and sediment sources of DOC are not substantially depleted over the timescale of this study (approximately 2 weeks). The model also makes the following noteworthy simplifications: (a) microbial and plant uptake are negligible, and microbial biomass is constant, (b) root exudates are negligible, (c) each layer is homogeneous (preferential flow paths are not represented).

The model was run in COMSOL (COMSOL AB, 2023) and was initialized by allowing the column to drain from a fully saturated state for 10 days. The upper boundary during this initialization step was treated as a no-flux boundary for all solutes except oxygen, which was able to exchange with the atmosphere via the convective-type boundary. The base was treated as a convective outflow boundary. Pore water concentrations were initialized with the same concentration as the groundwater end-member (Table 1). The 10-day initialization step was sufficient for all chemical species, including DOC and NH_4, to achieve new equilibrium concentrations reflective of respiration processes and DOC solubilization in the unsaturated pores. The final saturation state and pore water concentrations were then used as initial conditions for the model of the experiment. Hydraulic head was specified at the base of the column to follow linear changes similar to the experiment. For chemical transport,

Table 2
Aqueous-Phase Reactions Included in the Numerical Model, Their Stoichiometry, and Kinetic Rate Terms

Reaction	Stoichiometry	Monod term
Aerobic respiration	$(CH_2O)_x(NH_4^+)_y + xO_2 \rightarrow xCO_2 + yNH_4^+ + xH_2O$	$\Gamma_{\mathrm{AR}} = v_{\mathrm{AR}} B \left(\frac{c_{\mathrm{DOC}}}{k_{s,\mathrm{DOC}} + c_{\mathrm{DOC}}}\right) \left(\frac{c_{\mathrm{O_2}}}{k_{s,\mathrm{O_2}} + c_{\mathrm{O_2}}}\right)$
Nitrification	$O_2 + 1/2NH_4^+ \rightarrow 1/2NO_3^- + H^+ + 1/2H_2O$	$\Gamma_{\mathrm{NIT}} = v_{\mathrm{NIT}} B \left(\frac{c_{\mathrm{NH_4}}}{k_{s,\mathrm{NH_4}} + c_{\mathrm{NH_4}}}\right) \left(\frac{c_{\mathrm{O_2}}}{k_{s,\mathrm{O_2}} + c_{\mathrm{O_2}}}\right)$
Denitrification Step 1	$(CH_2O)_x(NH_4^+)_y + 2xNO_3^- \rightarrow xCO_2 + yNH_4^+ + xH_2O + 2xNO_2^-$	$\Gamma_{\mathrm{DN1}} = v_{\mathrm{DN1}} B \left(\frac{c_{\mathrm{DOC}}}{k_{s,\mathrm{DOC}} + c_{\mathrm{DOC}}}\right) \left(\frac{c_{\mathrm{NO_3}}}{k_{s,\mathrm{NO_3}} + c_{\mathrm{NO_3}}}\right) \left(\frac{k_{I,\mathrm{O_2}}}{k_{I,\mathrm{O_2}} + c_{\mathrm{O_2}}}\right)$
Denitrification Step 2	$(CH_2O)_x(NH_4^+)_y + 4/3xNO_2^- \rightarrow xCO_2 + yNH_4^+ + 5/3xH_2O + 2/3xN_2$	$\Gamma_{\mathrm{DN2}} = v_{\mathrm{DN2}} B \left(\frac{c_{\mathrm{DOC}}}{k_{s,\mathrm{DOC}} + c_{\mathrm{DOC}}}\right) \left(\frac{c_{\mathrm{NO_2}}}{k_{s,\mathrm{NO_2}} + c_{\mathrm{NO_2}}}\right) \left(\frac{k_{I,\mathrm{O_2}}}{k_{I,\mathrm{O_2}} + c_{\mathrm{O_2}}}\right)$

Table 3
Soil Characteristics in the Column

Layer	Depth (cm)	Oxidizable C (%)	OM (%)	d_{10} (mm)	d_{50} (mm)	K_s (m/s)
Organic II	0–10	4.62	8.89	0.08	0.45	1.63×10^{-4}
Organic I	10–30	3.31	8.01	0.08	0.54	1.24×10^{-4}
Mineral II	30–60	0.35	2.48	0.07	0.23	1.26×10^{-4}
Mineral I	60–100	0.86	1.32	0.35	1.42	2.73×10^{-3}

Note. d_{10} is the Tenth percentile grain diameter, d_{50} is the median grain diameter, and K_s is saturated hydraulic conductivity calculated using the Hazen method.

the base was treated as a mixed boundary. Concentrations were set to match groundwater in the tank (Table 1) except when water flowed out, at which time the base was treated as a convective outflow boundary. The top was treated as a no-flow boundary for water and solutes (excluding oxygen), except during the seawater flood, when a constant mass flux of water was prescribed at the top and solute concentrations were set to seawater values. Sides were treated as no-flow boundaries for both water and solutes. The domain was discretized with regular quadrilateral elements with maximum height of 2.5 mm. We used an adaptive time step limited by the Courant number with a maximum step size of 0.001 days.

Some model parameters like maximum specific reaction rates were not measured directly but play an important role in the fate of NO_3. To constrain model parameters, we first performed a visual fit with trial and error. We then ran a set of 100 simulations where we randomly varied 7 model parameters selected from reported ranges (Table 1). We selected the 7 parameters based on the experience gained from our efforts to visually fit the experimental observations. We did not vary any hydrologic parameters such as permeability and van Genuchten constants because those parameters were set by soil texture and constrained by soil moisture and tensiometer data. We did vary the oxygen inhibition constant to allow for the possible co-respiration of oxygen and NO_3 in the single-porosity domain, as incubations of sandy marine sediments have shown that oxygen does not always act as a strong inhibitor (Gao et al., 2010), but the best-fitting model ultimately had strong inhibition (Table 1). We selected the best-fitting scenario from the 100 runs based on the root mean square error between modeled and measured NO_3 and DOC concentrations. The improvement over the best trial-and-error fit was modest. We did not attempt further calibration for a number of reasons. Most importantly, the data suggest preferential flow (e.g., along roots) that cannot easily be captured by our model. Furthermore, despite our effort to minimize sample volumes and limit sample frequency, it is possible that sampling occasionally disturbed steeper geochemical gradients, especially near boundaries between soil layers. Under these conditions, calibrating the model to the data may in fact lead to less realistic parameter values and would not substantially increase the insights from an uncalibrated model. The main goal of the model was to reproduce salient characteristics of the experimental observations through a relatively simple, scalable approach and then use the model to elucidate key transport processes in various soil layers during water table fluctuations.

3. Results

3.1. Soil Properties and Hydraulic Conductivity

The percent of organic matter is lowest at the base of the column and increases upward through the organic soils at the surface (Table 3). The saturated hydraulic conductivity from grain size analysis varies from 2.73×10^{-3} m/s to 1.24×10^{-4} m/s across the four layers. The effective saturated hydraulic conductivity from infiltration data was estimated to be 1.6×10^{-5} m/s, which is an order of magnitude less than estimates from grain size analysis but still within the expected range for the sediment textures in the column (Freeze & Cherry, 1979). The saturated hydraulic conductivity of the mineral I layer (2.73×10^{-3} m/s) from the Hazen method agrees well with estimates for the unconfined aquifer at the site (Martínez-Pérez et al., 2022).

3.2. End-Member Chemistry

Groundwater that entered the column remained relatively stable in measured water quality parameters over the course of the experiment. Average recorded pH was 7.26 (standard deviation (σ) = 0.2), ORP was 167.6 mV (σ = 43 mV), and electrical conductivity was 978.8 μS/cm (σ = 3.2 μS/cm). Average dissolved oxygen concentration was 0.77 mg/L ($\sigma = 0.64$ mg/L). Concentrations of NO_2-N, NH_4-N, and DOC were low (0.017, 0.01, and 1.46 mg/L, respectively), while NO_3-N was elevated (average of 16.5 mg/L, $\sigma = 0.6$ mg/L).

Seawater used to flood the column on day 14 had a recorded pH of 7.99, ORP of 101 mV, and specific conductivity of 55.35 mS/cm. The dissolved oxygen concentration is unknown but was likely saturated. NO_3-N was low (0.129 mg/L) compared to the groundwater end-member.

3.3. Observations Within the Column

Redox potential (Eh) measured with in-situ sensors displayed significant variability among layers. It remained stable in the uppermost organic layer, where the 10 cm sensor ranged between 71.3 and 386.2 mV (average of 146.0 mV), indicating slightly reducing conditions, despite the potential for rapid oxygen exchange with the atmosphere (Figure 3a). Low Eh values are consistent with the high concentrations of DOC in pore water at 10 cm (Figure 4d). In comparison, in the Mineral II layer at 40 cm, where soil saturation varied strongly over the experiment, Eh ranged widely (47.5–671.6 mV, average 561.7 mV; Figure 3c). Eh gradually declined while the water table was high (days 2–4 and 6–8) (Figure 3c). But Eh increased abruptly when the water table dropped below 40 cm at days 4 and 8, and then continued to increase more gradually toward a stable value above 600 mV over the following 1–2 days. The latter value suggests that the sensor was in contact with water in equilibrium with atmospheric oxygen (the sensor was located in the capillary fringe at the time). It is therefore clear that oxygen-rich air flowed down through the reducing topsoil at 10 cm (Figure 3a), entered the draining pores of the mineral layer, and increased the redox potential at 40 cm (Figure 3c). Interestingly, Eh did not vary strongly during fast water table fluctuations (day 11) or the seawater flood (day 14) at this depth (Figure 3c). At 100 cm, where the column was always saturated, the average Eh was 3.88 mV, and Eh varied between −239.2 and 524.7 mV as flow alternated between the influx of fresh groundwater and the discharge of column pore water (Figure 3d). Eh increased from −236 to 24.5 mV in response to the seawater flood on day 14 (Figure 3d).

NO_3 concentrations in the column were generally less than the concentration of incoming groundwater (Figure 4a). Concentrations decreased upwards as NO_3-rich groundwater interacted with shallower, organic-rich soils, except at the shallowest depth (10 cm), where concentration again increased (Figure 4a). Overall, the lowest average concentration of NO_3-N (5.92 mg/L) occurred at 40 cm. This depth also had depleted levels of NO_2-N (average of 0.03 mg/L) and NH_4-N (average of 0.12 mg/L) compared to greater depths and incoming groundwater. DOC concentrations increased steadily up the column from 2.02 mg/L at 100 cm to 71.9 mg/L at 10 cm (Figure 4d), consistent with a sediment source in the organic layers (and, to a lesser extent, the mineral layers) (Table 3). This, in combination with the pattern of NO_3 concentration, suggests NO_3 was removed by denitrification. The gradually declining trends in NO_3 concentration over time also imply substantial denitrification under saturated conditions (Figure 3c).

As the water table rose on day 2 and 6, NO_3 concentrations tended to increase abruptly, as NO_3-rich groundwater flooded the column, and then decline under stagnant conditions, presumably due to denitrification (dashed lines in Figures 3a, 3b, and 3d). For example, at 25 cm (Figures 3b and 5a), NO_3-N concentrations rose rapidly by 7.41 mg/L on day 2 as the water table rose. Concentrations then gradually fell over 2 days by 16.7 mg/L before the water table fell again on day 4. This gradual decline during the 2 days before the water table fell can only be explained by chemical transformation and not advection or mixing of new water sources, as no flow would have been occurring while the water table was static. Also during days 2–4, NH_4-N concentrations gradually rose by 0.79 mg/L (Figure 5b). Conversely, NO_2-N concentrations remained unchanged during the first day (from day 2 until day 3) and then increased by 0.19 mg/L from day 3–4. In contrast, at 40 and 55 cm within the Mineral II layer, when the water table rose on days 2 and 6, NO_3 concentrations initially increased for a few hours, presumably due to nitrification driven by trapped oxygen. Then, concentrations gradually declined (as at 25 cm) due to denitrification (dashed lines in Figure 3c). These two sampling points were located in the capillary fringe when the water table was low. Additionally, NH_4 concentrations in the Mineral II layer did not increase as much as at 25 cm under sustained saturated conditions (compare Figures 5b and 5e).

DOC dynamics over sustained 2-day cycles were most evident in the shallow, organic layers (Figures 6a and 6b) where the organic matter in the soil was greatest. DOC concentrations rapidly decreased as the water table rose and remained at a similar concentration during static conditions (Figures 6a and 6b). When the water table fell, DOC concentrations increased again as DOC was transported down into deeper layers with flowing groundwater. The responses across both 2-day fluctuations were similar but with a decreasing trend as the experiment

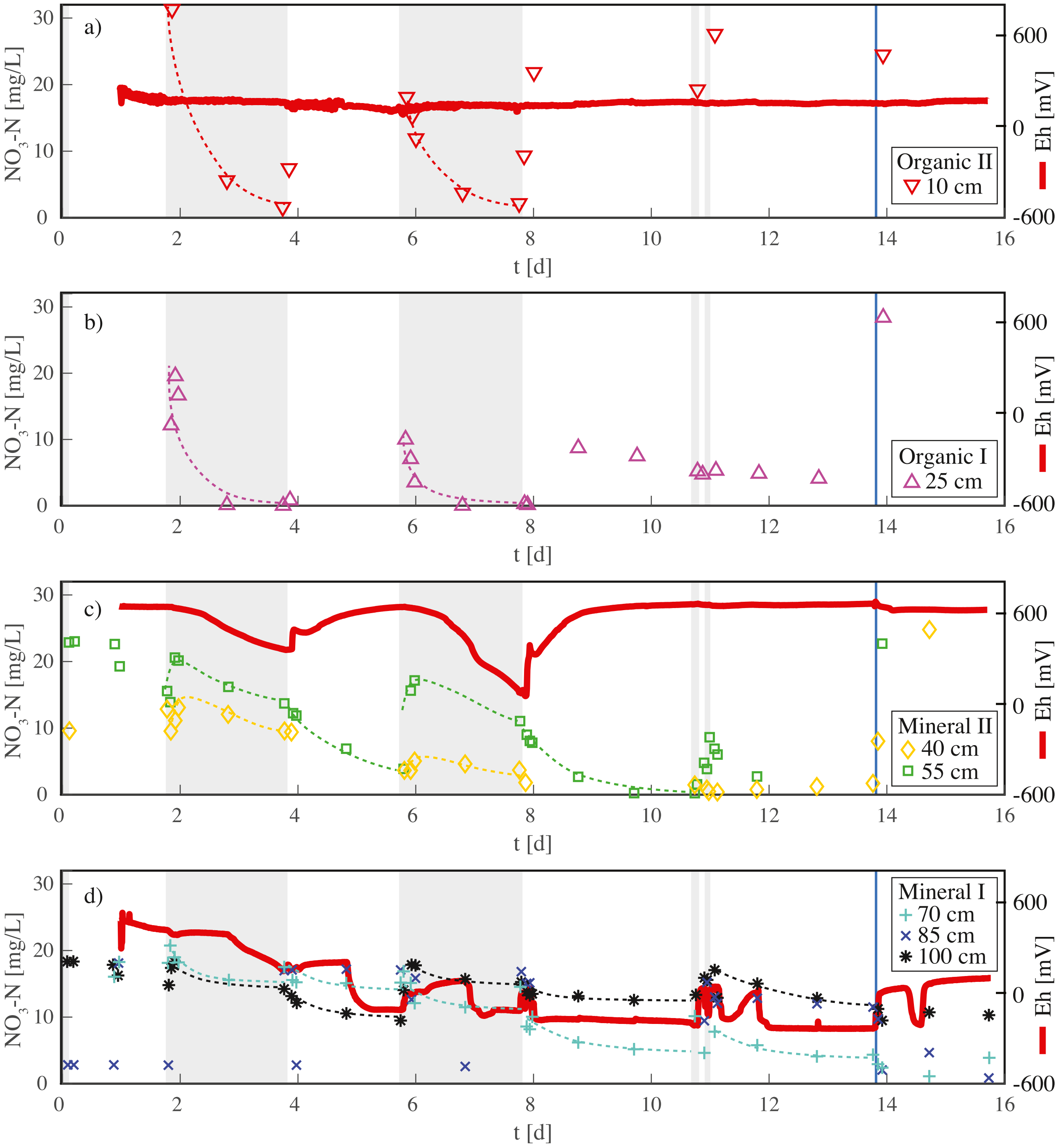

Figure 3. NO_3-N (symbols, left axis) over time at each sampled depth and continuous redox potential (Eh) (red curves, measured at 10, 40 and 100 cm) in the four layers of the column (a–d). Gray shading denotes a high water table (Figure 2c). Blue shading on day 14 represents seawater flooding the top of the column (NO_3-N concentration in seawater = 0.129 mg/L).

progressed. For example, at 10 cm, the concentration immediately after the water table rose on day 6 was 14.95 mg/L less than the concentration immediately after the water table rose on day 2 (Figure 6a). Similarly, there was a 14.25 mg/L difference in DOC concentrations when the water table was lowered on days 4 and 8 (Figure 6a). This gradually declining pattern occurred in the deeper layers as well, although it was not as dramatic due to the already low DOC concentrations there (Figures 6d–6g).

During faster, half-day fluctuations (day 11), NO_3 fluctuations still occurred at most depths (Figure 3). Some of the largest observed fluctuations (differences of ~6–7 mg/L) occurred in the mineral layers (e.g., at 55 and 85 cm)

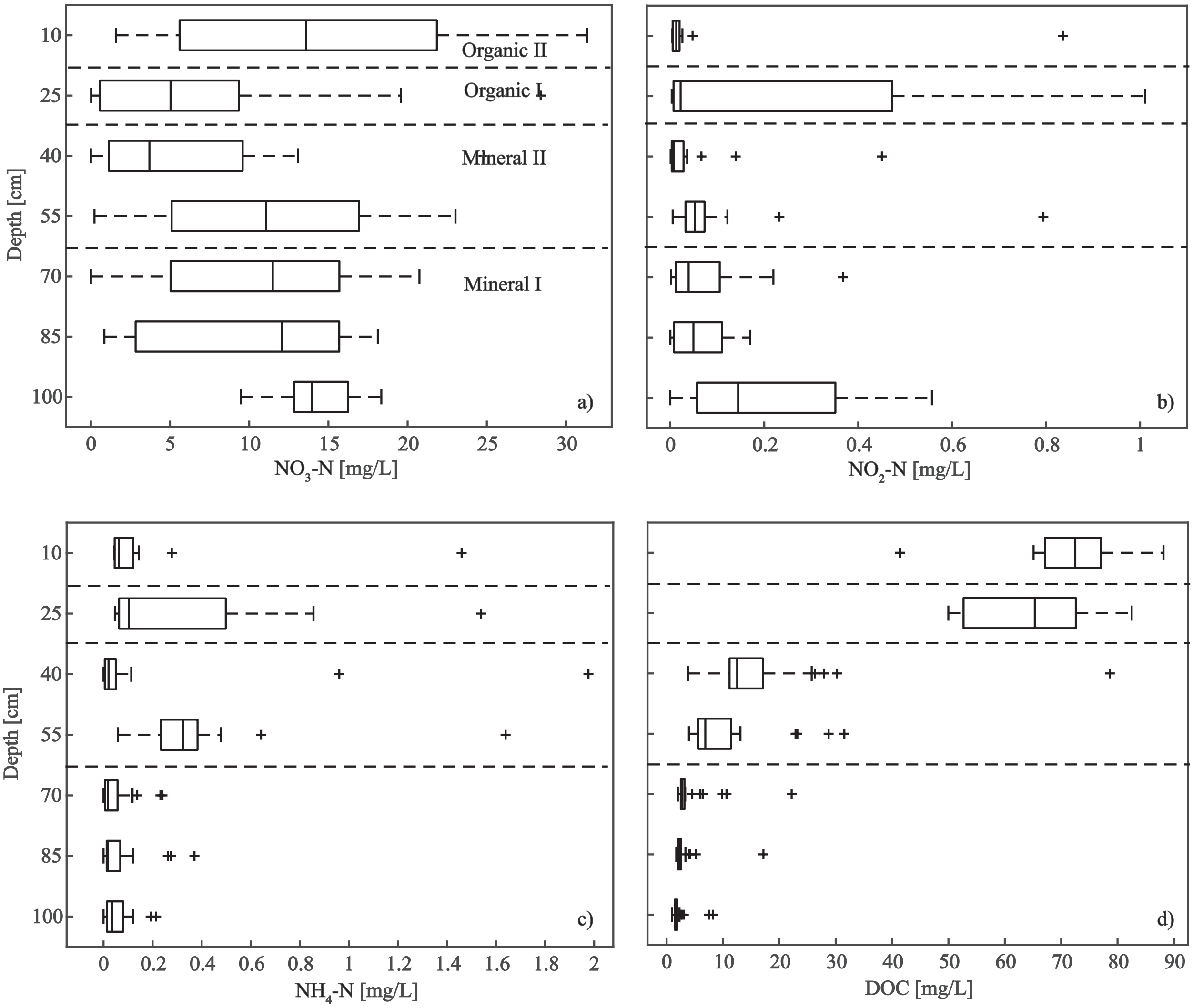

Figure 4. Distribution of measured NO_3-N (a), NO_2-N (b), NH_4-N (c), and dissolved organic carbon (d) in pore water at each depth. Dashed lines represent soil layer boundaries. Note the difference in horizontal axis for NO_3-N, NH_4-N, and NO_2-N. Samples below detection are shown as 0 mg/L. The only potential sources of N and C in the column are incoming groundwater (which is similar to the chemistry at 100 cm) and organic matter in the soils. Concentrations that exceed the concentration at 100 cm indicate a source, and those less than the concentration at 100 cm indicate a sink.

near the top of the saturated zone (Figures 3c and 3d). Meanwhile, NH_4 and NO_2 were more stable (Figure 5e). For example, at 40 cm (Figures 5d and 5e), NO_3-N concentrations varied by 1.07 mg/L over the half-day fluctuations (Figure 5d), while NH_4-N and NO_2-N only varied by 0.02 and <0.01 mg/L, respectively (Figure 5e). DOC concentrations were generally relatively stable over the short, half-day fluctuations, except at 25 cm in the bottom of the Organic I layer, near the interface with mineral layers, where fluctuations on the order of 15 mg/L were evident (Figure 5c).

The seawater flood on day 14 introduced oxic water that was relatively low in NO_3-N (0.129 mg/L) and moderate in DOC (6.21 mg/L). As this water infiltrated the column, NH_4, NO_3, and NO_2 concentrations increased rapidly at most depths (Figures 3 and 5, Figure S2 in Supporting Information S1). The largest abrupt increases in NH_4 occurred at 25 and 40 cm (Figure 5e). At 25 cm in the organic-rich soils, the NH_4-N concentration was 0.05 mg/L before the flood and 1.54 mg/L 2 hr following the flood (Figure 6). At 55 cm in the mineral II layer, an abrupt increase was not detected during the flood, but a substantial increase to 1.64 mg/L was measured 19 hr later (not shown). The largest observed increase in NO_3-N occurred at 25 cm (Figure 5b), with a concentration of 4.10 mg/L before the flood and 28.4 mg/L 2 hr after the flood. Unfortunately, no final samples were collected from this depth to ascertain whether concentrations remained elevated in the 1–2 days that followed. At a depth of 40 cm, the

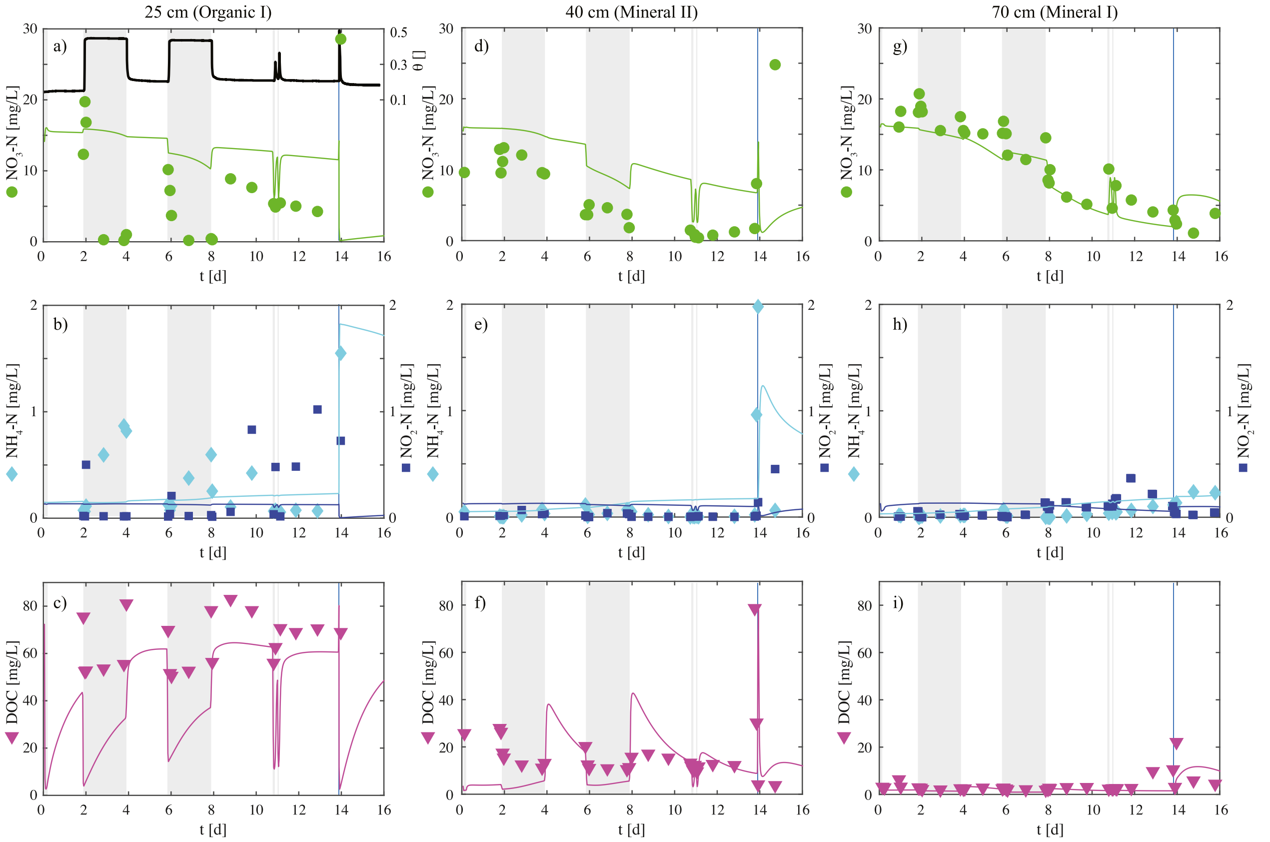

Figure 5. Measured (points) and modeled (solid curves) N species concentrations (upper two rows) and dissolved organic carbon concentrations (lower row) at three representative depths in the column: 25 cm (a–c), 40 cm (d–f), and 70 cm (g–i). Continuous volumetric water content (θ) measured with the soil moisture sensor at 20 cm is also shown for comparison in panel (a) (black solid line).

NO_3-N concentration similarly increased the day after the flood to 24.8 mg/L (Figure 5d). NO_2-N concentrations remained low during the flood, with increases of less than 0.78 mg/L and 0.006 mg/L in the organic layers at 10 cm (not shown) and 25 cm depths (Figure 5b), respectively. In the more mineral layers immediately below, when final samples were collected on day 15, the NO_2-N concentrations had increased from 0.14 to 0.45 mg/L at 40 cm (Figure 5e) and from 0.23 to 0.79 mg/L at 55 cm (not shown). Meanwhile, the concentration of NH_4-N at 40 cm decreased back to near pre-flood values (0.06 mg/L) (Figure 5e, Figure S2 in Supporting Information S1).

Also during the seawater flood, DOC concentrations in shallow soils at 10 cm decreased to a minimum of 41.4 mg/L, as seawater of low DOC concentration infiltrated (Figure 6a). At 40 cm, the DOC concentration decreased from 78.6 mg/L 2 hr before the flood to 4.1 mg/L 2 hr after the flood (Figure 6c). At 55 cm, there was an increase to 31.5 mg/L during the flood and partial recovery to 22.9 mg/L 2 hr after the flood (Figure 6c). At 70 cm and 85 cm, there was an initial decrease in DOC concentration followed by a spike, 2 hr after the flood, to 17.2 and 22.2 mg/L, respectively, as DOC-rich pore water from organic soils entered the deeper saturated zone (Figure 6d). At 100 cm, there was a spike in DOC concentration to 8.3 mg/L during the flood and 7.5 mg/L 2 hr after the flooding event (Figure 6d).

3.4. Model-Based Insights

The numerical model captures several key behaviors prior to flooding, including: (a) consumption of oxygen followed by NO_3 when the water table remained high for multiple days (days 2–4 and 6–8 in Figure 7a), which is consistent with the observed decline in redox potential near the water table at 40 cm (Figure 3c) and decline in NO_3 concentrations at most depths (Figures 3a–3c), (b) the gradual decline in NO_3 near the interface between organic and mineral layers, particularly evident at 40 cm (Figures 3c, 5d, and 5g), leading to the development of a depleted zone near the middle of the column (Figures 4a, 5d, and 7b), (c) the gradual accumulation of NH_4,

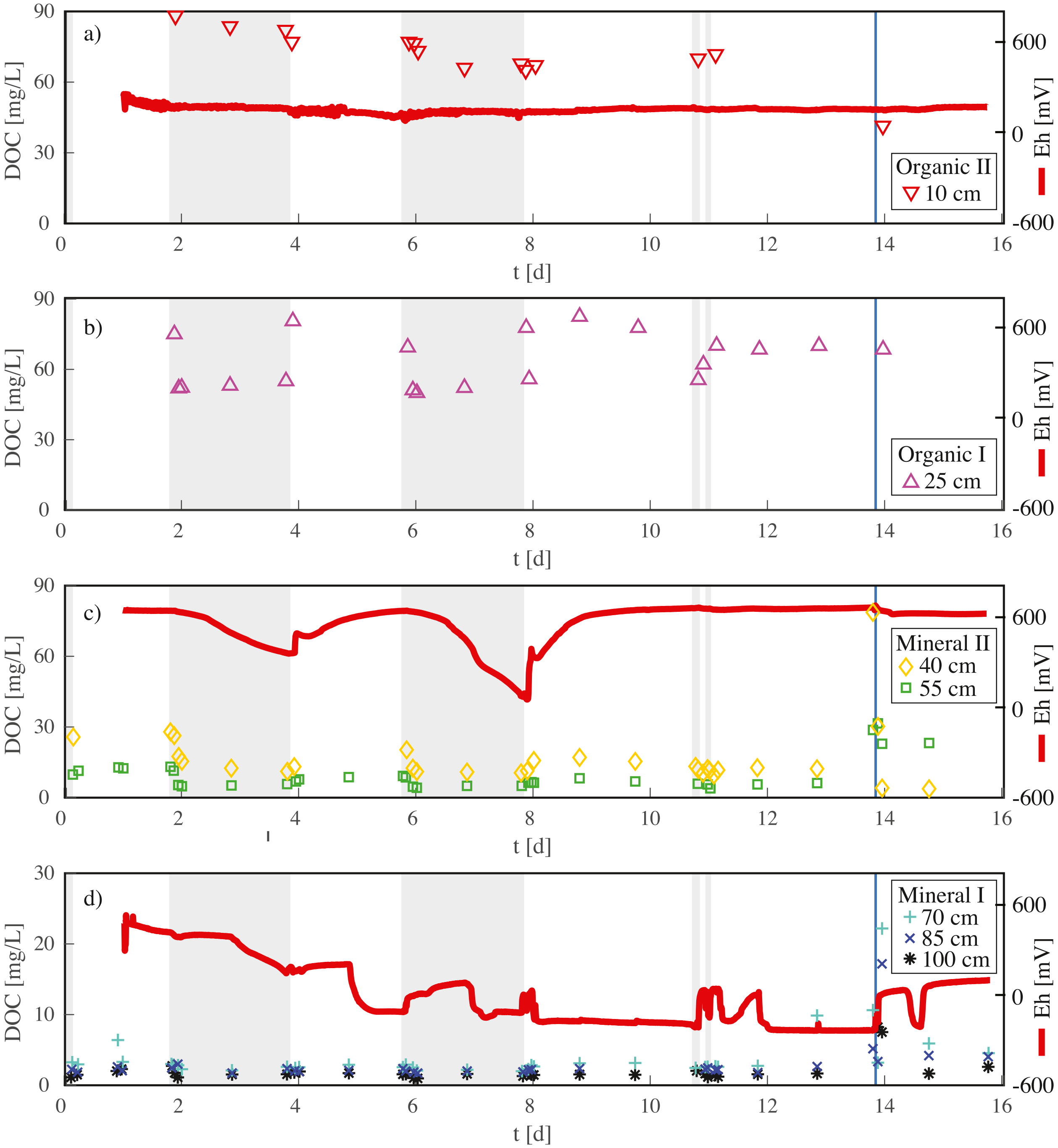

Figure 6. Measured dissolved organic carbon (DOC) concentrations (symbols, left axis) over time at each sampled depth and continuous redox potential (Eh) (red curves, measured at 10, 40, and 100 cm depths) in the four layers of the column (a–d). Gray shading denotes a high water table (Figure 2c). Blue shading on day 14 represents the seawater flood where Mediterranean water was introduced to the top of the column (DOC concentration in seawater = 0.9 mg/L). Note smaller concentration range for deeper locations in panel (d).

particularly in shallow organic layers (Figures 5b, 5e, 5h, and 7c), and strong gradients in DOC concentration across soil layers (Figures 5c, 5f, 5i, and 7d).

During the model flood event, a large pool of NH_4-N desorbed from soils as saline water moved downward, leading to peak pore water concentrations on the order of 2 mg/L, consistent with observations (Figures 5e and 7c). As infiltrating seawater mixed with pore water that had been held in the vadose zone under tension, dissolved oxygen, NO_3, and DOC migrated downward by advection in the model (Figures 7a, 7b, and 7d). Salinity-

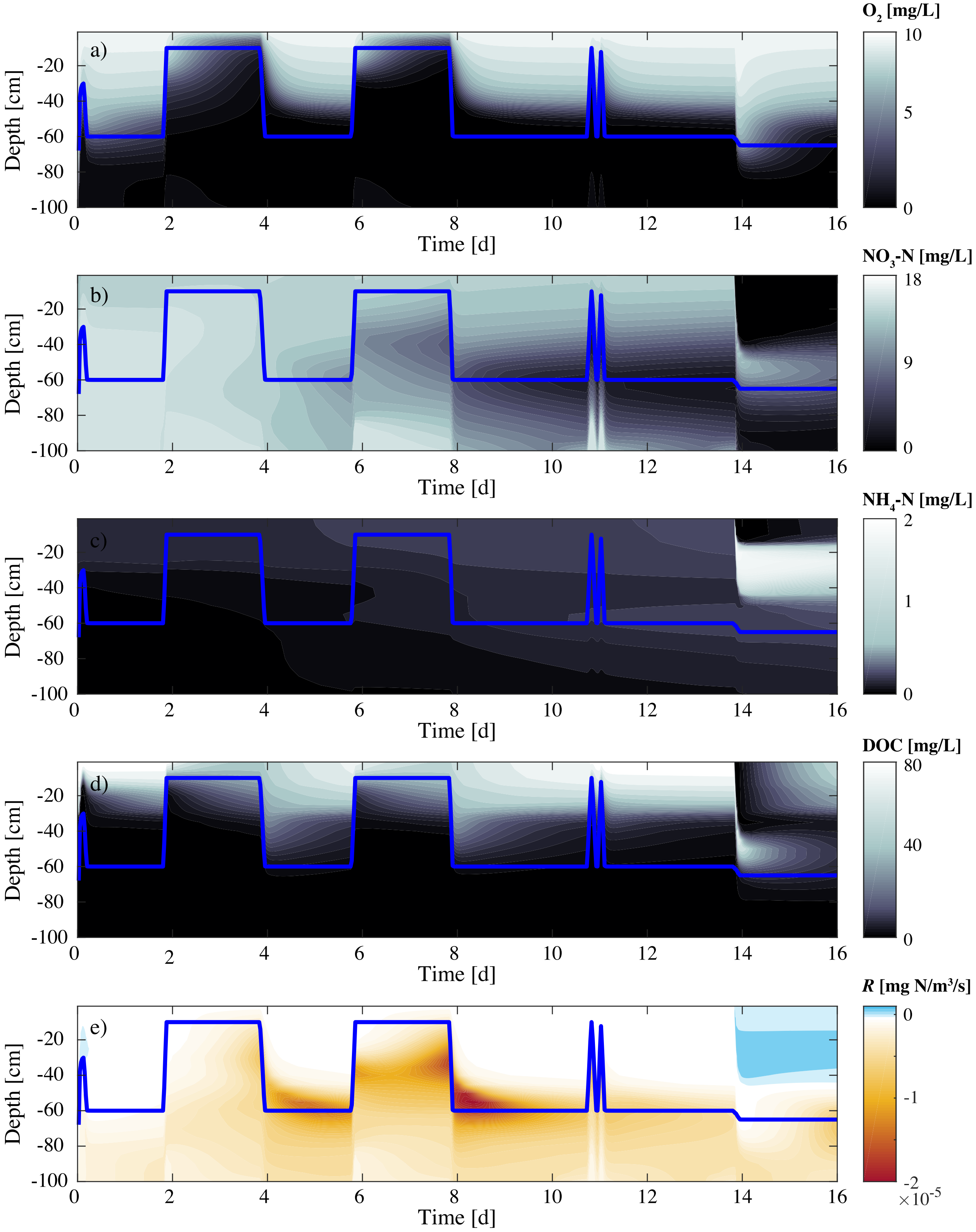

Figure 7. Depth-time contours of modeled concentrations in panels (a) dissolved oxygen (O_2), (b) NO_3-N, (c) NH_4-N, and (d) dissolved organic carbon, along with (e) the rate of production or removal of NO_3-N (*R*) due to nitrification and denitrification. Blue line indicates the position of the water table. Flooding with seawater occurred at the end of day 13.

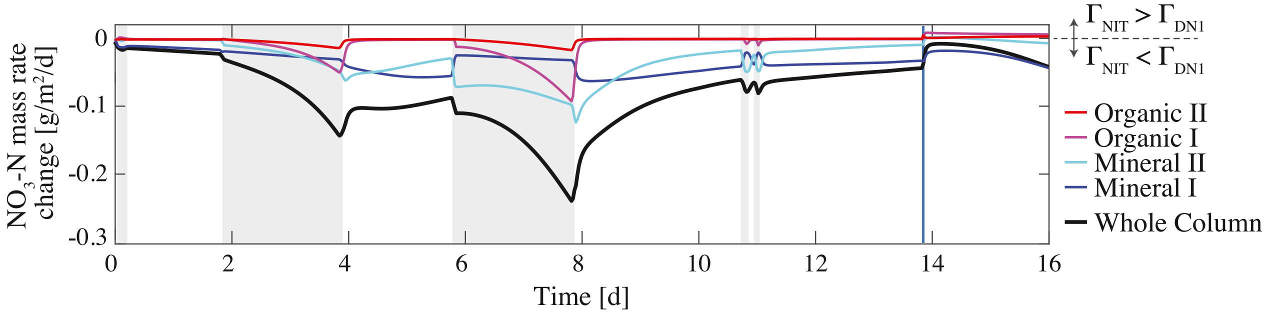

Figure 8. Spatially integrated rates of NO_3-N production or removal (the imbalance between nitrification and denitrification) in each soil layer (colors) and the overall column (black curve) within the model. Gray shading denotes a high water table. Blue shading on day 14 represents the flood when seawater was introduced to the top of the column.

dependent sorption of DOC was not needed to produce a downward pulse of DOC within reasonable range of observations at most depths (e.g., Figure 5f) because the pore water in the vadose zone had large concentrations of DOC (>50 mg/L), though the model did underestimate the DOC pulse at 70 cm (Figure 5i).

Modeled reaction rates varied strongly in both space and time due to variations in the supply of oxygen (controlled by saturation) and DOC (released by shallow soil layers) (Figure 7e). In general, the unsaturated zone above the capillary fringe was not a strong sink for NO_3 due to abundant oxygen (Figure 7a) and NH_4 from the mineralization of organic N (Figure 7c) that drove nitrification. A hotspot of nitrification also occurred in the unsaturated zone following the seawater flood due to the pulse of oxygen and NH_4 from above (Figure 7e). The Organic I layer (15–30 cm) acted as a hotspot of denitrification and thus a sink of NO_3 whenever the water table rose and saturated the pore space because of the local supply of DOC from organic matter and restricted supply of oxygen from the atmosphere (Figure 7e). When the water table fell, the draining Mineral II layer (30–60 cm) continued to act as a denitrification hotspot until DOC from shallower layers was consumed (Figure 7d) and concentrations of oxygen increased (Figure 7a). A similar behavior occurred almost 2 days after the seawater flood as reducing conditions re-established in the capillary fringe (Figure 7e).

Integrating the rates of NO_3 production and removal over the entire column, denitrification always outpaced nitrification (black line, Figure 8). The NO_3 removal rate increased substantially during periods with a prolongingly elevated water table (days 2–4 and 6–8), as saturated organic-rich soil layers switched from aerobic to anaerobic conditions. These model results are consistent with downward trends in Eh at 40 cm during the same periods (Figure 3c). Interestingly, modeled NO_3 removal rates barely fluctuated at all when the water table rose and fell over shorter timescales on day 11 (Figure 8), also consistent with stable Eh sensor data (Figure 3c). Saturated conditions in the more organic-rich soils did not persist long enough to consume oxygen and enable rapid denitrification (Figure 7a). During the flood event, the column remained an overall net sink for NO_3, but a weaker one (Figure 8). The downward-moving pulse of inorganic N from shallow soil layers lingered near the bottom of the vadose zone (Figure 7b). There, denitrification effectively removed much of the NO_3 within 2 days, despite the influx of oxygen with flood waters, due to the abundance of DOC in shallow soils.

It is clear, however, that the model does not capture some of the features observed in the experiment (Figure 5). Perhaps the most significant one is the non-monotonic variation in Eh (and, presumably, oxygen) at shallower depths (Figure 3), which helps explain the poorer agreement between measured and modeled N species at 25 and 40 cm (Figure 5). The observations suggest that oxygen-rich air flowed through the reducing topsoil layer into the draining pore space when the water table was lowered, where it caused an increase in redox potential (Figure 6c). This multiphase flow behavior could perhaps be reproduced with the Richard equation, but we would need a multi-continuum approach to maintain the observed anaerobic conditions in the topsoil as air flows through it. Aerobic and anaerobic respiration sites can co-exist in organic-rich soils due to strong gradients in oxygen and carbon at the pore scale (Borer et al., 2018) and have also been invoked in permeable coastal sands to explain high denitrification rates under bulk oxic conditions (Santos et al., 2012). Such pore-scale heterogeneities are clearly present within the column. Wang et al. (2022) incorporated them in reactive transport models by means of multi-rate-mass-transfer approaches to illustrate geochemical localization (i.e., the occurrence of local micro environments favoring reactions that would not occur in a fully mixed environments). However, representing them in

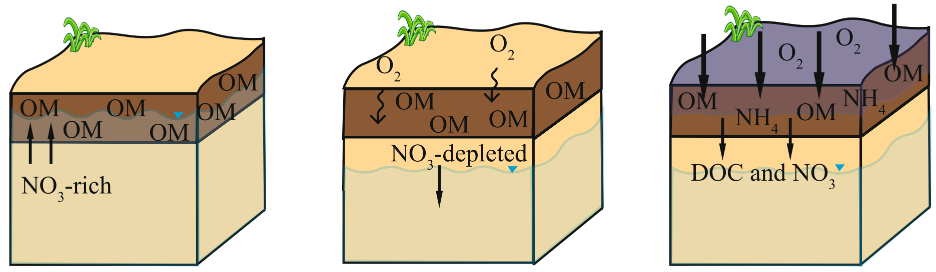

	Elevated Water Table	*Low Water Table*	*Seawater Flood*
Oxygen supply	Decreases in saturated pores	Increases as pores drain	Increases with infiltration of oxygen rich seawater
Carbon supply	Increases with saturation of organic rich soils	Decreases as pores drain	Increases with infiltration of carbon rich soil water from above
Inorganic N supply	NO_3 immedietly increases with upward flow of contaminated groundwater	Decreases as pores drain	NH_4 and NO_3 are mobilized from shallow soils
Dominant reactions	Aerobic respiration followed by denitrification and N mineralization	Nitrification	Desorption, aerobic respiration, nitrification, and denitrification
Calculated change in NO_3-N mass in column per unit area (this study)	day 6-8: -1.12 g/m^2 (Supporting Information Table S1)		day 13-15: +3.16 g/m^2 (Supporting Information Table S2)

Figure 9. Conceptual diagram of hydrologic processes that affect N fate near the water table and dominant reactions. Equations for nitrification and denitrification are available in Table 2.

our model would have required a large number of additional parameters to represent water retention and reactivity in immobile regions in each layer and would have transformed the modeling exercise into a fitting exercise, which was not our goal. What is clear is that a Richards approach is not sufficient to reproduce our observation. Still, the geochemical model appears adequate, as the model reproduces overall trends. The model approach also has the advantage of being tractable for larger-scale studies of N transport in coastal systems (e.g., Heiss et al., 2017; Li et al., 2024). The main limitation is that the model produces high concentrations of oxygen throughout the vadose zone when the water table drops, even in organic-rich soils, which prevents a rapid switch to denitrification and drawdown of NO_3 when the water table rises in organic-rich soils, as observed.

4. Discussion

Water table dynamics alter N fate in shallow aquifers by regulating the supply of both carbon and oxygen. The three main dynamics investigated in this experiment were: (a) elevating the water table, (b) lowering the water table, and (c) flooding the surface with seawater (Figure 9).

4.1. Biogeochemical Responses to Water Table Fluctuations

As the water table rose, the observed changes in NO_3 in the vadose zone were consistent with the upward transport of NO_3-rich groundwater from below, followed by fast removal throughout the column, but especially in organic-rich soils (Figure 3a). During periods with a sustained high water table (days 6–8 in Figure 10a), NO_3 concentrations in porewater samples decreased at every sampling depth except 85 cm. We assume that the primary removal process was denitrification and did not include other reactions that consume NO_3 in our model. Other pathways for NO_3 consumption include Anammox and dissimilatory nitrate reduction to ammonium (DNRA).

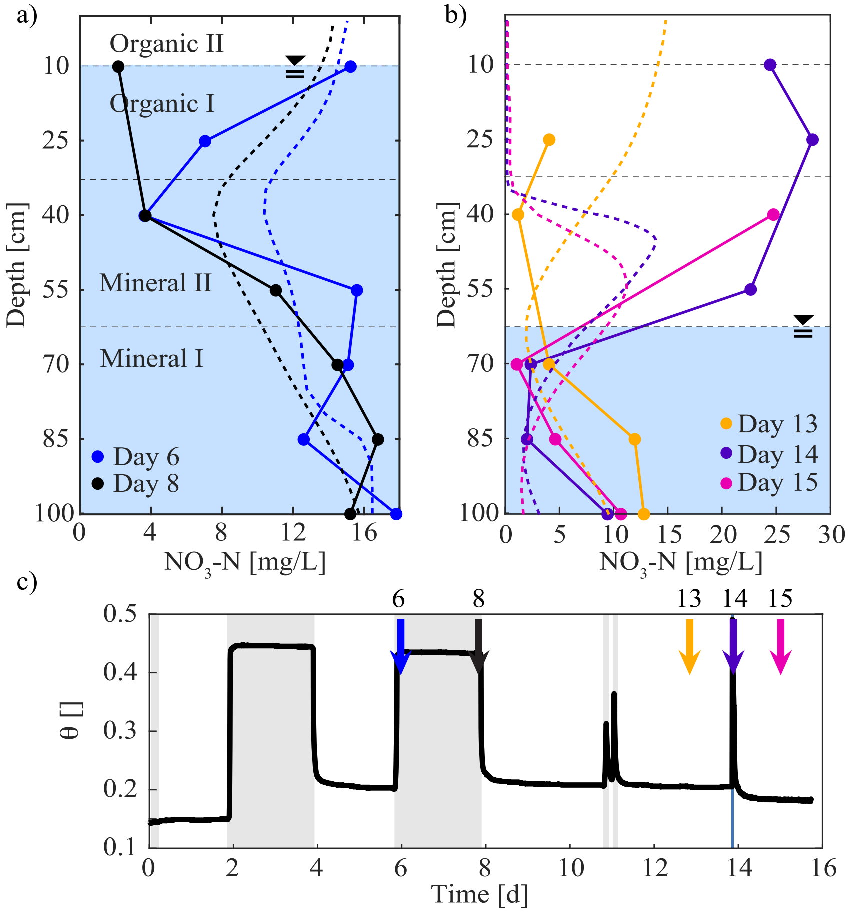

Figure 10. Depth profiles of NO_3-N over two dynamic periods: (a) days 6 and 8 (immediately after and two days after an increase in water table elevation), and (b) days 13–15 (1 day before, 2 hr after, and 1 day after the seawater flood). Circles indicate measurements, while dashed lines indicate model profiles. (c) Volumetric water content (θ) measured at 20 cm depth.

DNRA often occurs in extremely reducing environments (Buresh & Patrick, 1981). Given that our system is not extremely reducing near the water table (Eh was generally in the range of 300–600 mV at 40 cm), we do not attribute much NO_3 removal to DNRA. Observations and models both suggest that when the water table rises, the increase in saturation state reduces the supply of oxygen from the atmosphere to pore waters. Any remaining oxygen is rapidly consumed in microbial respiration (Figure 7a), allowing for microbes to use NO_3 as the electron acceptor (Rivett et al., 2008) (Figure 7b). The consumption of oxygen can be inferred not only from the consumption of NO_3 due to denitrification, which is inhibited by oxygen, but also from the decline in Eh at 40 cm depth (from 638.6 to 402.7 mV between days 2–4 and from 619.8 to 53.6 mV between days 6–8) (Figure 3). In fact, at this depth, denitrification did not start immediately. Instead, nitrification may have occurred during the first few hours (note dashed curves in Figure 3c), which probably reflects oxygen exchange from trapped air bubbles in the rising water table (Haberer et al., 2012). The fact that this early nitrification is not reflected in NH_4 concentrations probably suggests that most NH_4 is adsorbed.

When the water table fell, oxygen was rapidly drawn into the drained pores, as inferred from Eh measurements. Eh increased abruptly at 40 cm depth (days 4 and 8 in Figure 3c), even while it remained low in overlying topsoil at 10 cm depth. The downward flowing water that was replaced by air was also anoxic, as suggested by the reduction of NO_3 during the previous high water period (Figures 3a and 3b, days 2–4 and 6 to 8). This process is akin to "aquifer breathing"—the lowering of the water table creates the void space to be filled by air, much as the diaphragm creates void space in the lungs to suck air. Note that after an initially abrupt increase, it still takes almost a full day for the Eh sensor at 40 cm to equilibrate with atmospheric air (some 600 mV at days 5 and 9), which we assume reflects both oxygen diffusion within well connected pores in the mineral layers and the delayed downward flow of pore water. This oxygenation causes a switch from denitrification to aerobic respiration. Thus, lowering the water table tends to slow the rate of denitrification (Figure 8, days 4 and 8). Downward flow also slows denitrification by disconnecting groundwater from sediment sources of DOC in organic soils (McClain et al., 2003) (Figure 9). DOC that travels downward with groundwater may continue to drive NO_3 reduction at depth until DOC (or NO_3) are depleted.

In summary, when the water table rises into organic soil layers, the newly saturated vadose zone becomes a site of mixing between DOC from the local soils and NO_3 from rising groundwater, allowing a hotspot of denitrification (McClain et al., 2003) (Figure 9, Elevated Water Table condition). DOC concentrations initially decrease upon saturation as groundwater that is relatively depleted in DOC fills the pores, but then concentrations gradually recover over hours to days, as new DOC from the soil is leached into the porewater (Figure 7d). Since the supply of DOC commonly limits denitrification in NO_3-rich groundwater (Green et al., 2008; Tesoriero & Puckett, 2011), the mass loss of NO_3 under sustained saturated conditions should be greatest at shallower depths where more organic matter is present (DeSimone & Howes, 1998). It is then unsurprising that the greatest observed mass removal (as indicated by the change in concentration during the 2-day period when the water table remained high and flow was negligible) occurred at 10 cm, where DOC concentrations were greatest (Figure 10a). The model suggests a slightly deeper hotspot of removal around 30 cm, near the base of the Organic I layer where NO_3-rich groundwater interacts with DOC from organic-rich soils (Figure 7e). The difference may be due to model simplifications, including uniform bacterial biomass concentration. Biomass, and thus respiration rate, were likely greater at shallower depths with more DOC (e.g., Caruso et al., 2017; Monterroso et al., 2024), so including microbial growth and decay in the model would have increased oxygen and NO_3 depletion at shallower depths.

In total, we calculate from our observations that 1.12 g of NO_3-N were removed from groundwater over a 1 m^2 map-view area during the 50-cm sustained rise in the water table (Table S1 in Supporting Information S1), while the model suggests a total removal of 0.724. These calculations are based on the difference in total mass of NO_3-N in pore water at the start of the high water table condition on day 6 and the end of the high water table condition on day 8 (Figure 10a, Table S1 in Supporting Information S1). This experiment thus shows the potential for measurable and substantial mass reduction of NO_3 in groundwater through denitrification as the water table rises into organic layers with abundant DOC, consistent with field observations from Hefting et al. (2004). Water table cycles that saturate and drain organic-rich soils provide an important mechanism for supplying electron donors and acceptors to coastal aquifers, particularly where clean sand deposits are capped by organic-rich soils such as in salt marshes (Guimond & Tamborski, 2021).

4.2. Biogeochemical Responses to Seawater Flooding

In both observations and the model, the seawater flood mobilized large quantities of dissolved inorganic nitrogen in shallow soils, due to both the salinity-driven desorption of NH_4 from sediments and relatively conservative transport of pre-existing NO_3 in soil water. Saltwater has been shown to impact NH_4 through cation exchange in numerous studies, though salinity-dependent NH_4 sorption is rarely included in reactive transport models for coastal aquifers. Duckworth and Cresser (1991) showed an increase in NH_4 concentrations in pore water with the addition of NaCl to a maritime forest soils but concluded that this had little impact on NO_3 mobility over a 10 days experiment. Compton and Church (2011) used a series of soil column batch experiments to test the short- and long-term effects of sea salt on N cycling in coastal Oregon soils. They concluded that NH_4 was quickly mobilized with the addition of sea salt, but little NO_3 was released, similarly to Duckworth and Cresser (1991). However, during their month-long incubation Compton and Church (2011) found significant increases in both NH_4 and NO_3 and concluded that both incubation time and NaCl concentrations are an important factor in NO_3 mobilization. Our measurements during the seawater flood on day 14 (Figure 5) are consistent with these studies. We observed rapid NH_4 mobilization that could not be explained by advection alone and therefore chose to include salinity-dependent NH_4 sorption in the model. The pulse of NH_4 was accompanied by a pulse of NO_3, but the NO_3 pulse mainly originated from the pre-existing pool of NO_3 in soil water prior to the flood (Figure 7b).

While the pulse of NH_4 from sediments can be nitrified in the presence of oxygen in infiltrating seawater (Figure 9) (Duckworth & Cresser, 1991), NO_3 can subsequently be consumed by denitrification due to the presence of DOC from soils. Here, the spike in both NH_4 and NO_3 concentrations that traveled downward through the vadose zone did not contribute much N to the saturated zone (Figures 7b and 7c) for two reasons: (a) the flood was short, so the vadose zone never became fully saturated and the pulse of inorganic N lingered above the water table (Figure 7b), and (b) denitrification began to remove the lingering NO_3 near the water table in the day following the flood, thanks to an abundant supply of DOC (Figures 7d and 7e).

Comparing the NO_3-N profiles before and 1 day after the flood on days 13 and 15 (Figure 10b), we estimate that the mass of NO_3-N in pore water increased by 3.16 g over a 1 m^2 plan-view area (Figure 10b, Table S2 in Supporting Information S1). However, this value is particularly uncertain because the NO_3-N concentration at the shallowest depth (10 cm) was not measured prior to the flood. In comparison, the model suggests the mass of NO_3-N decreased by 0.767 g, due in part to flushing of NO_3-N from shallow soils into deeper zones of denitrification (Figure 10b).

The source of NO_3 to shallow groundwater during a flood should ultimately depend on this balance between advective travel time and denitrification rate (which is often limited by DOC) (Green et al., 2008), both of which vary with floods of different duration. As a test, we ran an additional computer simulation where we flooded the top of the column for 3 times longer (3 hr) (Figure 11). In this scenario, nearly the entire column saturated with oxygen-rich water around 14 days (Figure 11a). NO_3 from shallow soils flowed out through the base of the column (Figure 11b). In a natural system, this outflow would represent transport to greater depth, where denitrification could be limited if the sediment source of DOC is smaller there. NH_4 was again mobilized due to the salinity change. In this case, NH_4 entered the deepest mineral layer (compare Figures 7c and 11c). Nitrification dominated in shallow groundwater after the flood (Figure 11e). Therefore, the plume of NH_4 acted as a gradual (but small) source of NO_3 (Figure 11c). We interpret that longer floods have the potential to contribute more NO_3 to coastal aquifers by mobilizing both NO_3 and NH_4 in soils and promoting nitrification in shallow groundwater.

4.3. Implications

Dynamics in water table elevation and saturation state in coastal aquifers exert a dominant control on the sources and sinks of NO_3. Resulting NO_3 concentrations affect the quality of onshore groundwater, an important drinking water resource for coastal communities (Michael et al., 2017), but also offshore surface water, as submarine groundwater discharge delivers nutrients to the sea (Valiela et al., 1990). With greater proximity to the coast, the water table is more responsive to storm surge, wind, waves, and tides, and the land surface is more vulnerable to episodic flooding. Hydrologic forces are therefore expected to have an important influence on groundwater quality near the point of discharge. Water table fluctuations that bring NO_3 from groundwater in contact with DOC from soils over extended timescales (more than hours) ultimately improve shallow groundwater quality in areas where DOC availability tends to limit the reduction of groundwater NO_3. This is common in NO_3-contaminated aquifers (Seitzinger et al., 2006), including the one in this study, where molar C:N ratios in groundwater are small (Section 3.2). On the other hand, flooding soils with seawater may result in a net source of NO_3 to groundwater due to mobilization of N from soil pore water (Figures 9 and 11). This finding is consistent with field-based experiments that observed large pulses of dissolved inorganic N in coastal soils and wetlands inundated by seawater (Ardón et al., 2013; Jun et al., 2013).

The effects of water table fluctuations on N fate and transport should also vary with groundwater and soil chemistry. For example, in pristine coastal areas where the groundwater is low in NO_3, there is potential for both water table elevation and inundation to supply NO_3 to groundwater from the mineralization and mobilization of N in soils (Barnes et al., 2019; Wallace et al., 2020). Meanwhile, in locations where there are high populations and sewage systems, NO_3 concentrations in the vadose zone can exceed concentrations in the groundwater. Although a rising water table creates anoxic conditions and leads to denitrification with ample DOC, there might not be enough carbon to serve as an energy source in some coastal soils, and NO_3 would then enter the groundwater. As an example, in areas with abundant septic systems such as coastal Rhode Island (USA), the water table is rising on the order of 1 cm/y due to sea level rise (Cox et al., 2019). As tides and seasonal water table fluctuations bring groundwater in closer contact with septic systems over longer and more frequent intervals, the risk of N contamination to groundwater and surface water via submarine groundwater discharge increases.

Our continuous Eh data suggest reactions occur on timescales of hours to days when the water table changes (Figure 3). Therefore, fast water table fluctuations (as in day 11) transport chemical concentration gradients up and down without sufficient time to support a sustained source of DOC or consumption of oxygen, leading to modest changes in N (Figures 3 and 7b). Total mass sources and sinks of N therefore depend on a balance between the reaction timescale and the timescale of water table fluctuation (Ocampo et al., 2006; Oldham et al., 2013). We could not directly calculate mass changes from our observations over the faster fluctuations because pore water

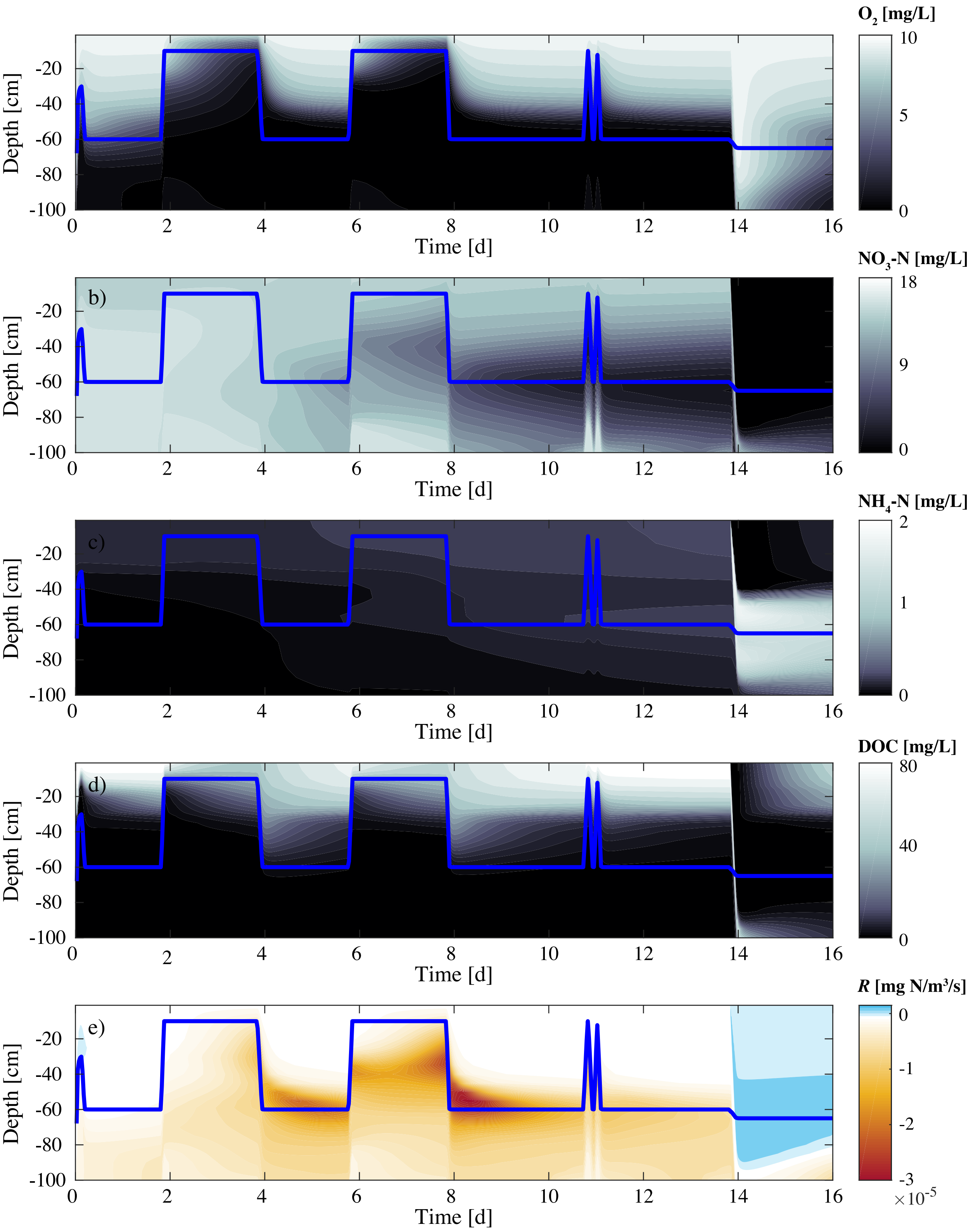

Figure 11. Depth-time contours of modeled concentrations and reaction rates for flood of longer (3-hr) duration: (a) dissolved oxygen (O_2), (b) NO_3-N, (c) NH_4-N, (d) dissolved organic carbon, and (e) the rate of production or removal of NO_3-N (R) due to nitrification and denitrification. Blue line indicates the position of the water table. Flooding with seawater occurred at the end of day 13.

samples could only be pulled semi-regularly, due to the slow sample production rates in the unsaturated zone. However, examining the more sustained fluctuations between days 2 and 4 and 6 and 8, NO_3 concentrations decreased steadily over the 2-day period when the water table was elevated (Figure 5). Pairing these along with our continuous redox measurements (Figure 3), Eh trended towards more reducing conditions over saturated 2-day periods at 40 cm, where denitrification was favored. At 10 cm, there was little change in the Eh measurements as the environment was already reducing, likely due to the high levels of DOC measured in the pore water samples. In contrast, during the rapid fluctuations that occurred on day 11, there were no noticeable fluctuations of Eh at 10 and 40 cm depths, implying that the soils needed to be saturated for longer periods of time before becoming more reducing (Figure 3). The pore water NO_3 concentrations were more variable from 55–100 cm depths, but model results show that these fluctuations can be explained by advection, specifically the displacement of steep concentration gradients in NO_3 in groundwater (Figure 7b).

5. Conclusions

The goal of this study was to investigate how water table dynamics influence the fate and transport of N in shallow coastal aquifers, with a focus on sites with excess groundwater NO_3. Our combined observations and model results show how a rising water table brings groundwater in contact with a fresh source of DOC in shallow, organic-rich soils, enhancing the removal of NO_3 through denitrification. In the topsoil, denitrification starts, as expected, with extremely fast rates as soon as the rising water table delivers NO_3. But in the mineral sediments beneath, which are more oxic than those above due to the flow of air through preferential pathways in the topsoil (the "aquifer breathing" effect), NO_3 concentrations increase in the initial hours, presumably due to nitrification. They then decline as the oxygen is consumed, as long as the high water table condition is sustained.

These observations lead to two important claims. First, perturbations that raise the water table for sustained periods may help remove NO_3 from contaminated coastal groundwater. Conversely, periods when seawater overtops and infiltrates the land surface may mobilize inorganic N in the soils, leading to the potential for tightly coupled nitrification-denitrification. In the absence of a sufficient carbon source, NO_3 may be transported into the aquifer, acting as a source of new contamination. Second, aquifers "breathe"—the fluctuating water table pushes and pulls air through preferential flow paths in otherwise reducing soils. This process might have been anticipated, as soils often contain a suite of preferential flow paths, but to our knowledge, it has not been demonstrated through controlled experiments. This breathing effect helps explain the frequent aerobic conditions in unconfined aquifers, despite the reducing conditions of most soils.

Data Availability Statement

All observational data and the input files for the numerical models are available in Roumelis (2024).

Acknowledgments
This study was supported by the National Science Foundation (EAR-1752995). Roumelis also received support from the Geological Society of America and the Association of Environmental and Engineering Geologists. Additional support came from project ConMimo (Spanish Research Agency, AEI, number TED2021-131188B-C31). We thank Lauren Decker, Hannah Field, and Rafael Bartrolí for their help with lab analyses and Alycia Insalaco for assistance with field work. We also thank the Associate Editor and three anonymous reviewers for constructive comments that improved the manuscript.

References

Abarca, E., Karam, H., Hemond, H. F., & Harvey, C. F. (2013). Transient groundwater dynamics in a coastal aquifer: The effects of tides, the lunar cycle, and the beach profile. *Water Resources Research*, *49*(5), 2473–2488. https://doi.org/10.1002/wrcr.20075

Abascal, E., Gómez-Coma, L., Ortiz, I., & Ortiz, A. (2022). Global diagnosis of nitrate pollution in groundwater and review of removal technologies. *Science of the Total Environment*, *810*, 152233. https://doi.org/10.1016/j.scitotenv.2021.152233

Almasri, M. N., & Ghabayen, S. M. (2008). Analysis of nitrate contamination of Gaza coastal aquifer, Palestine. *Journal of Hydrologic Engineering*, *13*(3), 132–140. https://doi.org/10.1061/(ASCE)1084-0699(2008)13:3(132)

Appelo, C. A. J., & Postma, D. (2004). *Geochemistry, groundwater and pollution*. CRC press.

Ardón, M., Morse, J. L., Colman, B. P., & Bernhardt, E. S. (2013). Drought-induced saltwater incursion leads to increased wetland nitrogen export. *Global Change Biology*, *19*(10), 2976–2985. https://doi.org/10.1111/gcb.12287

Arora, B., Dwivedi, D., Faybishenko, B., Jana, R. B., & Wainwright, H. M. (2019). Understanding and predicting vadose zone processes. *Reviews in Mineralogy and Geochemistry*, *85*(1), 303–328. https://doi.org/10.2138/rmg.2019.85.10

Baker, M. A., & Vervier, P. (2004). Hydrological variability, organic matter supply and denitrification in the Garonne River ecosystem. *Freshwater Biology*, *49*(2), 181–190. https://doi.org/10.1046/j.1365-2426.2003.01175.x

Barnes, R. T., Sawyer, A. H., Tight, D. M., Wallace, C. D., & Hastings, M. G. (2019). Hydrogeologic controls of surface water-groundwater nitrogen dynamics within a tidal freshwater zone. *Journal of Geophysical Research: Biogeosciences*, *124*(11), 3343–3355. https://doi.org/10.1029/2019JG005164

Befus, K. M., Barnard, P. L., Hoover, D. J., Finzi Hart, J. A., & Voss, C. I. (2020). Increasing threat of coastal groundwater hazards from sea-level rise in California. *Nature Climate Change*, *10*, 946–952. https://doi.org/10.1038/s41558-020-0874-1

Borer, B., Tecon, R., & Or, D. (2018). Spatial organization of bacterial populations in response to oxygen and carbon counter-gradients in pore networks. *Nature Communications*, *9*(1), 769. https://doi.org/10.1038/s41467-018-03187-y

Buresh, R. J., & Patrick, W. H. (1981). Nitrate reduction to ammonium and organic nitrogen in an estuarine sediment. *Soil Biology and Biochemistry*, *13*(4), 279–283. https://doi.org/10.1016/0038-0717(81)90063-8

Burkart, M. R., & Stoner, J. D. (2008). Chapter 7—Nitrogen in groundwater associated with agricultural systems. In J. L. Hatfield & R. F. Follett (Eds.), *Nitrogen in the environment* (2nd ed., pp. 177–202). Academic Press. https://doi.org/10.1016/B978-0-12-374347-3.00007-X

Cardenas, M. B., Bennett, P. C., Zamora, P. B., Befus, K. M., Rodolfo, R. S., Cabria, H. B., & Lapus, M. R. (2015). Devastation of aquifers from tsunami-like storm surge by supertyphoon haiyan. *Geophysical Research Letters*, *42*(8), 2844–2851. https://doi.org/10.1002/2015GL063418

Carretero, S. C., & Kruse, E. E. (2012). Relationship between precipitation and water-table fluctuation in a coastal dune aquifer: Northeastern coast of the Buenos Aires province, Argentina. *Hydrogeology Journal*, *20*(8), 1613–1621. https://doi.org/10.1007/s10040-012-0890-y

Caruso, A., Boano, F., Ridolfi, L., Chopp, D. L., & Packman, A. (2017). Biofilm-induced bioclogging produces sharp interfaces in hyporheic flow, redox conditions, and microbial community structure. *Geophysical Research Letters*, *44*(10), 4917–4925. https://doi.org/10.1002/2017GL073651

Cerdà-Domènech, M., Rodellas, V., Folch, A., & Garcia-Orellana, J. (2017). Constraining the temporal variations of Ra isotopes and Rn in the groundwater end-member: Implications for derived SGD estimates. *Science of the Total Environment*, *595*, 849–857. https://doi.org/10.1016/j.scitotenv.2017.03.005

Chang, S. W., & Clement, T. P. (2013). Laboratory and numerical investigation of transport processes occurring above and within a saltwater wedge. *Journal of Contaminant Hydrology*, *147*, 14–24. https://doi.org/10.1016/j.jconhyd.2013.02.005

Chen, J., Taniguchi, M., Liu, G., Miyaoka, K., Onodera, S., Tokunaga, T., & Fukushima, Y. (2007). Nitrate pollution of groundwater in the Yellow River delta, China. *Hydrogeology Journal*, *15*(8), 1605–1614. https://doi.org/10.1007/s10040-007-0196-7

Cirmo, C. P., & McDonnell, J. J. (1997). Linking the hydrologic and biogeochemical controls of nitrogen transport in near-stream zones of temperate-forested catchments: A review. *Journal of Hydrology*, *199*(1–2), 88–120. https://doi.org/10.1016/S0022-1694(96)03286-6

Compton, J. E., & Church, M. R. (2011). Salt additions alter short-term nitrogen and carbon mobilization in a coastal Oregon andisol. *Journal of Environmental Quality*, *40*(5), 1601–1606. https://doi.org/10.2134/jeq2011.0013

COMSOL AB. (2023). COMSOL Multiphysics® v. 6.2 [Software]. Retrieved from https://www.comsol.com/

Cox, A. H., Loomis, G. W., & Amador, J. A. (2019). Preliminary evidence that rising groundwater tables threaten coastal septic systems. *Journal of Sustainable Water in the Built Environment*, *5*(4), 04019007. https://doi.org/10.1061/JSWBAY.0000887

DeSimone, L. A., & Howes, B. L. (1998). Nitrogen transport and transformations in a shallow aquifer receiving wastewater discharge: A mass balance approach. *Water Resources Research*, *34*(2), 271–285. https://doi.org/10.1029/97WR03040

De Vos, B., Lettens, S., Muys, B., & Deckers, J. A. (2007). Walkley-Black analysis of forest soil organic carbon: Recovery, limitations and uncertainty. *Soil Use & Management*, *23*(3), 221–229. https://doi.org/10.1111/j.1475-2743.2007.00084.x

Duckworth, C. M. S., & Cresser, M. S. (1991). Factors influencing nitrogen retention in forest soils. *Environmental Pollution*, *72*(1), 1–21. https://doi.org/10.1016/0269-7491(91)90152-M

Fierer, N., & Schimel, J. P. (2002). Effects of drying–rewetting frequency on soil carbon and nitrogen transformations. *Soil Biology and Biochemistry*, *34*(6), 777–787. https://doi.org/10.1016/S0038-0717(02)00007-X

Folch, A., del Val, L., Luquot, L., Martínez-Pérez, L., Bellmunt, F., Le Lay, H., et al. (2020). Combining fiber optic DTS, cross-hole ERT and time-lapse induction logging to characterize and monitor a coastal aquifer. *Journal of Hydrology*, *588*, 125050. https://doi.org/10.1016/j.jhydrol.2020.125050

Folk, R. L., & Ward, W. C. (1957). Brazos River bar [Texas]; a study in the significance of grain size parameters. *Journal of Sedimentary Research*, *27*(1), 3–26. https://doi.org/10.1306/74D70646-2B21-11D7-8648000102C1865D

Freeze, R. A., & Cherry, J. A. (1979). *Groundwater*. Prentice Hall.

Gao, H., Schreiber, F., Collins, G., Jensen, M. M., Svitlica, O., Kostka, J. E., et al. (2010). Aerobic denitrification in permeable Wadden Sea sediments. *ISME Journal*, *4*(3), 417–426. https://doi.org/10.1038/ismej.2009.127

Gejl, R., Rygaard, M., Henriksen, H., Rasmussen, J., & Bjerg, P. (2019). Understanding the impacts of groundwater abstraction through long-term trends in water quality. *Water Research*, *156*, 241–251. https://doi.org/10.1016/j.watres.2019.02.026

Goyetche, T., Luquot, L., Carrera, J., Martínez-Pérez, L., & Folch, A. (2022). Identification and quantification of chemical reactions in a coastal aquifer to assess submarine groundwater discharge composition. *Science of the Total Environment*, *838*, 155978. https://doi.org/10.1016/j.scitotenv.2022.155978

Goyetche, T., Pool, M., Carrera, J., Diego-Feliu, M., Martínez-Pérez, L., Folch, A., & Luquot, L. (2023). Using the tidal method to develop a conceptual model and for hydraulic characterization at the Argentona research site, NE Spain. *Hydrogeology Journal*, *31*(8), 2099–2114. https://doi.org/10.1007/s10040-023-02730-6

Green, C. T., Puckett, L. J., Böhlke, J. K., Bekins, B. A., Phillips, S. P., Kauffman, L. J., et al. (2008). Limited occurrence of denitrification in four shallow aquifers in agricultural areas of the United States. *Journal of Environmental Quality*, *37*(3), 994–1009. https://doi.org/10.2134/jeq2006.0419

Greskowiak, J., Seibert, S. L., Post, V. E. A., & Massmann, G. (2023). Redox-zoning in high-energy subterranean estuaries as a function of storm floods, temperatures, seasonal groundwater recharge and morphodynamics. *Estuarine, Coastal and Shelf Science*, *290*, 108418. https://doi.org/10.1016/j.ecss.2023.108418

Guimond, J., & Tamborski, J. (2021). Salt marsh hydrogeology: A review. *Water*, *13*(4), 543. https://doi.org/10.3390/w13040543

Haberer, C. M., Rolle, M., Cirpka, O. A., & Grathwohl, P. (2012). Oxygen transfer in a fluctuating capillary fringe. *Vadose Zone Journal*, *11*(3). https://doi.org/10.2136/vzj2011.0056

Haberer, C. M., Rolle, M., Cirpka, O. A., & Grathwohl, P. (2015). Impact of heterogeneity on oxygen transfer in a fluctuating capillary fringe. *Ground Water*, *53*(1), 57–70. https://doi.org/10.1111/gwat.12149

Hazen, A. (1911). Dams on sand formations: Discussion. *Trans ASCE*, *73*, 199–203.

Heaton, T. H. E., Stuart, M. E., Sapiano, M., & Micallef Sultana, M. (2012). An isotope study of the sources of nitrate in Malta's groundwater. *Journal of Hydrology*, *414–415*, 244–254. https://doi.org/10.1016/j.jhydrol.2011.10.037

Hefting, M., Clément, J. C., Dowrick, D., Cosandey, A. C., Bernal, S., Cimpian, C., et al. (2004). Water table elevation controls on soil nitrogen cycling in riparian wetlands along a European climatic gradient. *Biogeochemistry*, *67*(1), 113–134. https://doi.org/10.1023/B:BIOG.0000015320.69868.33

Heiss, J. W., Mase, B., & Shen, C. (2022). Effects of future increases in tidal flooding on salinity and groundwater dynamics in coastal aquifers. *Water Resources Research*, *58*(12). https://doi.org/10.1029/2022WR033195

Heiss, J. W., Post, V. E. A., Laattoe, T., Russoniello, C. J., & Michael, H. A. (2017). Physical controls on biogeochemical processes in intertidal zones of beach aquifers. *Water Resources Research*, *53*(11), 9225–9244. https://doi.org/10.1002/2017WR021110

Hill, A. R., Devito, K. J., Campagnolo, S., & Sanmugadas, K. (2000). Subsurface denitrification in a forest riparian zone: Interactions between hydrology and supplies of nitrate and organic carbon. *Biogeochemistry*, *51*(2), 193–223. https://doi.org/10.1023/A:1006476514038

Holocher, J., Peeters, F., Aeschbach-Hertig, W., Hofer, M., Brennwald, M., Kinzelbach, W., & Kipfer, R. (2002). Experimental investigations on the formation of excess air in quasi-saturated porous media. *Geochimica et Cosmochimica Acta*, *66*(23), 4103–4117. https://doi.org/10.1016/S0016-7037(02)00992-4

Housego, R., Raubenheimer, B., Elgar, S., Cross, S., Legner, C., & Ryan, D. (2021). Coastal flooding generated by ocean wave- and surge-driven groundwater fluctuations on a sandy barrier island. *Journal of Hydrology*, *603*, 126920. https://doi.org/10.1016/j.jhydrol.2021.126920

Howarth, R. W., & Marino, R. (2006). Nitrogen as the limiting nutrient for eutrophication in coastal marine ecosystems: Evolving views over three decades. *Limnology & Oceanography*, *51*(1, Part 2), 364–376. https://doi.org/10.4319/lo.2006.51.1_part_2.0364

Isla, F. I., Quiroz Londoño, O. M., & Cortizo, L. C. (2018). Groundwater characteristics within loessic deposits: The coastal springs of Los Acantilados, Mar del Plata, Argentina. *Environmental Earth Sciences*, *77*(17), 610. https://doi.org/10.1007/s12665-018-7766-y

Jardine, P. M., Dunnivant, F. M., Selim, H. M., & McCarthy, J. F. (1992). Comparison of models for describing the transport of dissolved organic carbon in aquifer columns. *Soil Science Society of America Journal*, *56*, 393–401.

Jasechko, S., Perrone, D., Seybold, H., Fan, Y., & Kirchner, J. W. (2020). Groundwater level observations in 250,000 coastal US wells reveal scope of potential seawater intrusion. *Nature Communications*, *11*(1), 3229. https://doi.org/10.1038/s41467-020-17038-2

Johannes, R. (1980). The ecological significance of the submarine discharge of groundwater. *Marine Ecology Progress Series*, *3*, 365–373. https://doi.org/10.3354/meps003365

Jost, D., Haberer, C. M., Grathwohl, P., Winter, J., & Gallert, C. (2015). Oxygen transfer in a fluctuating capillary fringe: Impact of microbial respiratory activity. *Vadose Zone Journal*, *14*(5), 1–14. https://doi.org/10.2136/vzj2014.04.0039

Jun, M., Altor, A. E., & Craft, C. B. (2013). Effects of increased salinity and inundation on inorganic nitrogen exchange and phosphorus sorption by tidal freshwater floodplain forest soils, Georgia (USA). *Estuaries and Coasts*, *36*(3), 508–518. https://doi.org/10.1007/s12237-012-9499-6

Kliewer, B. A., & Gilliam, J. W. (1995). Water table management effects on denitrification and nitrous oxide evolution. *Soil Science Society of America Journal*, *59*(6), 1694–1701. https://doi.org/10.2136/sssaj1995.03615995005900060027x

Kwon, E., Park, J., Park, W.-B., Kang, B.-R., & Woo, N. C. (2021). Nitrate contamination of coastal groundwater: Sources and transport mechanisms along a volcanic aquifer. *Science of the Total Environment*, *768*, 145204. https://doi.org/10.1016/j.scitotenv.2021.145204

Li, B., Li, Z., Zheng, J., Jiang, P., Holmquist, J., Regier, P. J., et al. (2024). Integrated effects of site hydrology and vegetation on exchange fluxes and nutrient cycling at a coastal terrestrial-aquatic interface. *Water Resources Research*, *60*(6), e2023WR035580. https://doi.org/10.1029/2023WR035580

Martínez-Pérez, L., Luquot, L., Carrera, J., Marazuela, M. A., Goyetche, T., Pool, M., et al. (2022). A multidisciplinary approach to characterizing coastal alluvial aquifers to improve understanding of seawater intrusion and submarine groundwater discharge. *Journal of Hydrology*, *607*, 127510. https://doi.org/10.1016/j.jhydrol.2022.127510

McClain, M. E., Boyer, E. W., Dent, C. L., Gergel, S. E., Grimm, N. B., Groffman, P. M., et al. (2003). Biogeochemical hot spots and hot moments at the interface of terrestrial and aquatic ecosystems. *Ecosystems*, *6*(4), 301–312. https://doi.org/10.1007/s10021-003-0161-9

Michael, H. A., Post, V. E. A., Wilson, A. M., & Werner, A. D. (2017). Science, society, and the coastal groundwater squeeze. *Water Resources Research*, *53*(4), 2610–2617. https://doi.org/10.1002/2017WR020851

Monterroso, H., Widdowson, M. A., Lotts, W. S., Strom, K. B., & Hester, E. T. (2024). Effects of boundary hydraulics, dissolved oxygen, and dissolved organic carbon on growth and death dynamics of aerobic microbes in riverbed dune-induced hyporheic zones. *Science of the Total Environment*, *906*, 167401. https://doi.org/10.1016/j.scitotenv.2023.167401

Mostaza-Colado, D., Carreño-Conde, F., Rasines-Ladero, R., & Iepure, S. (2018). Hydrogeochemical characterization of a shallow alluvial aquifer: 1 baseline for groundwater quality assessment and resource management. *Science of the Total Environment*, *639*, 1110–1125. https://doi.org/10.1016/j.scitotenv.2018.05.236

Nielsen, P., Aseervatham, R., Fenton, J. D., & Perrochet, P. (1997). Groundwater waves in aquifers of intermediate depths. *Advances in Water Resources*, *20*(1), 37–43. https://doi.org/10.1016/S0309-1708(96)00015-2

Nolan, B. T. (2001). Relating nitrogen sources and aquifer susceptibility to nitrate in shallow ground waters of the United States. *Ground Water*, *39*(2), 290–299. https://doi.org/10.1111/j.1745-6584.2001.tb02311.x

Ocampo, C. J., Oldham, C. E., & Sivapalan, M. (2006). Nitrate attenuation in agricultural catchments: Shifting balances between transport and reaction: Shifting Balances in Nitrate Attenuation. *Water Resources Research*, *42*(1). https://doi.org/10.1029/2004WR003773

Oldham, C. E., Farrow, D. E., & Peiffer, S. (2013). A generalized Damköhler number for classifying material processing in hydrological systems. *Hydrology and Earth System Sciences*, *17*(3), 1133–1148. https://doi.org/10.5194/hess-17-1133-2013

Pabich, W. J., Valiela, I., & Hemond, H. F. (2001). Relationship between DOC concentration and vadose zone thickness and depth below water table in groundwater of Cape Cod, U.S.A. *Biogeochemistry*, *55*(3), 247–268. https://doi.org/10.1023/A:1011842918260

Pal, L., Stres, B., Danevčič, T., Leskovec, S., & Mandic-Mulec, I. (2010). Transformations of mineral nitrogen applied to peat soil during sequential oxic/anoxic cycling. *Soil Biology and Biochemistry*, *42*(8), 1338–1346. https://doi.org/10.1016/j.soilbio.2010.03.013

Palacios, A., Ledo, J. J., Linde, N., Luquot, L., Bellmunt, F., Folch, A., et al. (2020). Time-lapse cross-hole electrical resistivity tomography (CHERT) for monitoring seawater intrusion dynamics in a Mediterranean aquifer. *Hydrology and Earth System Sciences*, *24*(4), 2121–2139. https://doi.org/10.5194/hess-24-2121-2020

Pronk, G. J., Mellage, A., Milojevic, T., Smeaton, C. M., Engel, K., Neufeld, J. D., et al. (2020). Carbon turnover and microbial activity in an artificial soil under imposed cyclic drainage and imbibition. *Vadose Zone Journal*, *19*(1), e20021. https://doi.org/10.1002/vzj2.20021

Rezanezhad, F., Couture, R.-M., Kovac, R., O'Connell, D., & Van Cappellen, P. (2014). Water table fluctuations and soil biogeochemistry: An experimental approach using an automated soil column system. *Journal of Hydrology*, *509*, 245–256. https://doi.org/10.1016/j.jhydrol.2013.11.036

Rivett, M. O., Buss, S. R., Morgan, P., Smith, J. W. N., & Bemment, C. D. (2008). Nitrate attenuation in groundwater: A review of biogeochemical controlling processes. *Water Research*, *42*(16), 4215–4232. https://doi.org/10.1016/j.watres.2008.07.020

Robertson, G. P., & Groffman, P. M. (2007). Nitrogen Transformations. In *Soil microbiology, ecology and biochemistry* (pp. 341–364). Elsevier. https://doi.org/10.1016/B978-0-08-047514-1.50017-2

Rodríguez-Escales, P., Folch, A., van Breukelen, B. M., Vidal-Gavbilan, G., & Sanchez-Vila, X. (2016). Modeling long term Enhanced in situ Biodenitrification and induced heterogeneity in column experiments under different feeding strategies. *Journal of Hydrology*, *538*, 127–137. https://doi.org/10.1016/j.jhydrol.2016.04.012

Roumelis, C. (2023). *Water table fluctuations control nitrate sources and sinks in a mediterranean coastal aquifer* (M.S. Thesis). The Ohio State University.

Roumelis, C. (2024). Geophysical and geochemical data corresponding to "Water Table Fluctuations Control Nitrate Sources and Sinks in a Mediterranean Coastal Aquifer [Dataset]. *HydroShare*. Retrieved from https://doi.org/10.4211/hs.b04e4524648a456ebaf68c60a18550ee

Rühle, F. A., von Netzer, F., Lueders, T., & Stumpp, C. (2015). Response of Transport Parameters and Sediment Microbiota to Water Table Fluctuations in Laboratory Columns. *Vadose Zone Journal*, *14*(5), 1–12. https://doi.org/10.2136/vzj2014.09.0116

Santos, I. R., Eyre, B. D., & Glud, R. N. (2012). Influence of porewater advection on denitrification in carbonate sands: Evidence from repacked sediment column experiments. *Geochimica et Cosmochimica Acta*, *96*, 247–258. https://doi.org/10.1016/j.gca.2012.08.018

Seitzinger, S., Harrison, J. A., Bohlke, J. K., Bouwman, A. F., Lowrance, R., Peterson, B., et al. (2006). Denitrification across landscapes and waterscapes: A synthesis. *Ecological Applications*, *16*(6), 2064–2090. https://doi.org/10.1890/1051-0761(2006)016[2064:dalawa]2.0.co;2

Shah, D. B., & Coulman, G. A. (1978). Kinetics of nitrification and denitrification reactions. *Biotechnology and Bioengineering*, *20*(1), 43–72. https://doi.org/10.1002/bit.260200105

Sinke, A. J. C., Dury, O., & Zobrist, J. (1998). Effects of a fluctuating water table: Column study on redox dynamics and fate of some organic pollutants. *Journal of Contaminant Hydrology*, *33*(1–2), 231–246. https://doi.org/10.1016/S0169-7722(98)00072-2

Smith, R. L., & Duff, J. H. (1988). Denitrification in a Sand and Gravel Aquifer. *Applied and Environmental Microbiology*, *54*(5), 1071–1078. https://doi.org/10.1128/aem.54.5.1071-1078.1988

Sobczak, W. V., Findlay, S., & Dye, S. (2003). Relationships between DOC bioavailability and nitrate removal in an upland stream: An experimental approach. *Biogeochemistry*, *62*(3), 309–327. https://doi.org/10.1023/A:1021192631423

Spalding, R. F., & Exner, M. E. (1993). Occurrence of Nitrate in Groundwater—A Review. *Journal of Environmental Quality*, *22*(3), 392–402. https://doi.org/10.2134/jeq1993.00472425002200030002x

Squeo, F. A., Aravena, R., Aguirre, E., Pollastri, A., Jorquera, C. B., & Ehleringer, J. R. (2006). Groundwater dynamics in a coastal aquifer in north-central Chile: Implications for groundwater recharge in an arid ecosystem. *Journal of Arid Environments*, *67*(2), 240–254. https://doi.org/10.1016/j.jaridenv.2006.02.012

Strebel, O., Duynisveld, W. H. M., & Böttcher, J. (1989). Nitrate pollution of groundwater in western Europe. *Agriculture, Ecosystems & Environment*, *26*(3–4), 189–214. https://doi.org/10.1016/0167-8809(89)90013-3

Tesoriero, A. J., & Puckett, L. J. (2011). O_2 reduction and denitrification rates in shallow aquifers. *Water Resources Research*, *47*(12). https://doi.org/10.1029/2011WR010471

Tran, T. H. H., Kim, S. H., Jo, H. Y., Chung, J., & Lee, S. (2022). Transient behavior of arsenic in vadose zone under alternating wet and dry conditions: A comparative soil column study. *Journal of Hazardous Materials*, *422*, 126957. https://doi.org/10.1016/j.jhazmat.2021.126957

Trglavcnik, V., Morrow, D., Weber, K. P., Li, L., & Robinson, C. E. (2018). Analysis of tide and offshore storm-induced water table fluctuations for structural characterization of a coastal island aquifer. *Water Resources Research*, *54*(4), 2749–2767. https://doi.org/10.1002/2017WR020975

Valiela, I., Costa, J., Foreman, K., Teal, J. M., Howes, B., & Aubrey, D. (1990). Transport of groundwater-borne nutrients from watersheds and their effects on coastal waters. *Biogeochemistry*, *10*(3), 177–197. https://doi.org/10.1007/BF00003143

de Voogt, P. (Ed.). (2017). *Reviews of environmental contamination and toxicology* (Vol. 242). Springer International Publishing. https://doi.org/10.1007/978-3-319-51243-3

Wallace, C. D., Sawyer, A. H., Barnes, R. T., Soltanian, M. R., Gabor, R. S., Wilkins, M. J., & Moore, M. T. (2020). A model analysis of the tidal engine that drives nitrogen cycling in coastal riparian aquifers. *Water Resources Research*, *55*(4). https://doi.org/10.1029/2019WR025662

Wang, J., Carrera, J., Saaltink, M. W., & Valhondo, C. (2022). On the localization of chemical reactions in multicontinuum media. *Advances in Water Resources*, *167*, 104286. https://doi.org/10.1016/j.advwatres.2022.104286

Williams, M. D., & Oostrom, M. (2000). Oxygenation of anoxic water in a fluctuating water table system: An experimental and numerical study. *Journal of Hydrology*, *230*(1–2), 70–85. https://doi.org/10.1016/s0022-1694(00)00172-4

Zhang, Z., & Furman, A. (2021). Redox dynamics at a dynamic capillary fringe for nitrogen cycling in a sandy column. *Journal of Hydrology*, *603*, 126899. https://doi.org/10.1016/j.jhydrol.2021.126899